

1 **Capturing the interplay of membrane lipids and structural transitions in human ABCA7**

2 Le Thi My Le¹†, James R. Thompson¹†, Sepehr Dehghani-Ghahnaviyeh², Shashank Pant^{2,#}, Phuoc
3 X. Dang¹, Takahisa Kanikeyo³, Emad Tajkhorshid² & Amer Alam^{1,*}

4

5 ¹The Hormel Institute, University of Minnesota, Austin, Minnesota 59912

6 ² Theoretical and Computational Biophysics Group, NIH Center for Macromolecular
7 Modeling and Bioinformatics, Beckman Institute for Advanced Science and Technology,
8 Department of Biochemistry, and Center for Biophysics and Quantitative Biology,
9 University of Illinois at Urbana-Champaign, Urbana, IL, USA

10 ³Department of Neuroscience, Mayo Clinic, Jacksonville, Florida 32224

11 †These authors contributed equally to this work

12 # Current affiliation: Loxo Oncology at Lilly., Louisville, CO 80027, USA

13 *Address correspondence to: Amer Alam, PhD, aalam@umn.edu

14 **Abstract**

15 Phospholipid extrusion by ABC subfamily A (ABCA) exporters is central to cellular physiology,
16 although the specifics of the underlying substrate interactions and transport mechanisms remain
17 poorly resolved at the molecular level. Here we report cryo-EM structures of lipid-embedded
18 human ABCA7 in an open state and a nucleotide-bound, closed state at resolutions between 3.6-
19 4.0 Å. The former reveals an ordered patch of bilayer lipids traversing the transmembrane domain
20 (TMD), while the latter reveals a lipid-free, closed TMD with a small extracellular opening. These
21 structures offer a structural framework for both substrate entry and exit from the ABCA7 TMD
22 and highlight conserved rigid-body motions that underlie the associated conformational

23 transitions. Combined with functional analysis and molecular dynamics (MD) simulations, our
24 data also shed light on lipid partitioning into the ABCA7 TMD and localized membrane
25 perturbations that underlie ABCA7 function and have broader implications for other ABCA family
26 transporters.

27

28 **Introduction**

29 ABCA family exporters mediate efflux of phospholipids and sterols from cells,
30 contributing to membrane homeostasis, bilayer structure and asymmetry, and the formation of
31 serum lipoproteins, among other key physiological processes¹. Their dysfunction therefore
32 underlies several human diseases²⁻⁴. The molecular details governing the ABCA exporter substrate
33 transport cycle are not fully resolved. To fill this knowledge gap, here we present the structural
34 and functional analysis of human ABCA7, whose dysfunction has been strongly linked to
35 Alzheimer's Disease (AD)⁵⁻¹², in a lipid environment. Deficient ABCA7 activity leads to
36 alterations in both brain lipid profiles and fatty acid and phospholipid biosynthetic pathways¹³,
37 impaired memory, and reduced immune responses^{14,15}. Both *in vitro* lipid flipping¹⁶ and lipid
38 extrusion to apolipoproteins by cells over-expressing ABCA7¹⁷ have been demonstrated, although
39 the correlation between the two processes, if any, remains unclear. To date, no direct structural
40 information exists for ABCA7. Understanding the molecular details of the ABCA7 transport cycle
41 and how its dysfunction alters inflammatory and immune responses, lipid homeostasis, and
42 phagocytosis, which all contribute to AD progression¹⁸⁻²², may therefore pave the way for novel
43 therapeutics for AD.

44 ABCA7 encodes a 2146 amino acid membrane transporter found in many tissues and
45 blood, hippocampal neurons, macrophages, and microglia^{23,24}. Like the phospholipid and sterol

46 exporter ABCA1 and retinal importer ABCA4, with which it shares 54% and 59% sequence
47 similarity, respectively, ABCA7 comprises two halves assembled as a full transporter. Each half
48 consists of a TMD, with the first two transmembrane helices (TMs) of each separated by a large
49 extracellular domain (ECD), and a nucleotide binding domain (NBD) attached to a cytoplasmic
50 regulatory domain (RD). To visualize its ATP-dependent conformational cycle in a lipid
51 environment, we resolved the structures of human ABCA7 in multiple conformations in lipid and
52 detergent environments using cryo-EM and probed its lipid interactions using ATPase assays and
53 MD simulations. Our data allow us to directly visualize lipid partitioning into the TMDs and the
54 associated conformational changes in ABCA7 that provide insights into its mechanisms of
55 substrate entry and export that likely hold true for other members of the ABCA family.

56 **Results**

57 **Dependence of ABCA7 ATPase activity on its lipid environment**

58 Human ABCA7 expressed in a tetracycline inducible stable HEK293 cell line was
59 reconstituted in liposomes and nanodiscs comprising 80% brain polar lipids (BPL) and 20%
60 cholesterol (Chol) and its ATPase activity was measured (Figure 1A, Figure S1A). Although ATP
61 hydrolysis was slowest in nanodiscs, it followed Michaelis-Menten kinetics similar to ABCA7 in
62 detergent or liposomes comprising the same lipid/cholesterol composition and Michaelis constant
63 (K_M) values for all three were in the 0.5-0.8 mM range. ATPase rates for a hydrolysis-deficient
64 mutant carrying E965Q and E1951Q substitutions (ABCA7_{EQ}) were drastically reduced compared
65 to wildtype in both nanodiscs and detergents, demonstrating that the observed activity was specific
66 (Figure S1A).

67 To analyze the effect of different lipid headgroups on ATPase activity, we compared
68 ATPase rates of ABCA7 in BPL/Chol nanodiscs to those in which BPL was replaced by either

69 brain polar phosphatidylethanolamine (PE), phosphatidylserine (PS) or phosphatidylcholine (PC)
70 as well 100% BPL nanodiscs. As seen in Figure 1B, ATPase rates were highest in PE and PS
71 nanodiscs followed by 100% BPL nanodiscs lacking cholesterol and, lastly, PC nanodiscs that
72 showed a marginal increase. These results largely match previous findings¹⁶, although differences
73 exist in extent of ATPase rate stimulation that are likely due to the divergent lipid formulations
74 used for reconstitution. Overall, they demonstrate that lipids modulate ABCA7 activity in a species
75 dependent manner and that cholesterol has an inhibitory effect on ATPase activity of ABCA7.

76 **Cryo-EM structures of ABCA7 in nanodiscs reveal an asymmetric, open TMD**

77 To visualize ABCA7 in a lipid environment, we determined its cryo-EM structures in
78 BPL/Chol nanodiscs (ABCA7_{BPL}) at 3.6 Å resolution (Figure 1C, Figure S1B-E). Despite the
79 addition of the non-hydrolysable ATP analog adenosine-5'-o-(3-thio-triphosphate) (ATP γ S), the
80 transporter adopted an open conformation with separated NBDs and a wide open TMD pathway.
81 We observed density features consistent with a patch of ordered lipids from both bilayer leaflets
82 traversing the width of TMD as expanded upon below. A second, higher-resolution 3D class
83 displayed more complete density for the ECD tunnel region but comparatively lower quality of
84 EM density for TMD2-NBD2 and the entire RD, indicating greater conformational disorder, which
85 was therefore not analyzed further (Figure S1D-E). Analysis of TMD-ECD interfaces in the
86 ABCA7_{BPL} structures revealed more extensive contacts between the ECD and TMD1 (buried
87 surface area (BSA) of 790 Å²) compared to TMD2 (330 Å² BSA). Both TMD1 and TMD2 made
88 contacts with the opposite ECD subunits, leading to a domain swapped arrangement. The TMD1-
89 ECD2 interface (BSA 565 Å²) was significantly larger than that of TMD1-ECD1 (BSA 223 Å²)
90 and both interfaces comprised an extensive network of polar and electrostatic interactions. The RD

91 adopted a domain-swapped arrangement similar to that in ABCA4 structures²⁵, with RD1 and RD2
92 associated with the opposite NBDs. To see whether structural changes could rationalize the
93 enhanced ATPase activity observed in ABCA7_{PE} compared to ABCA7_{BPL}, we also determined the
94 cryo-EM structure of the former to 4.0 Å resolution (Figure 1D, Figure S2). Interestingly, both
95 structures were nearly identical to each other (r.m.s.d 0.31Å), although only a single high
96 resolution 3D class was resolved for ABCA7_{PE} (Figure S2). Compared to ABCA7_{BPL}, density for
97 TMD lipids was more homogenous, despite its comparatively lower resolution, as described
98 below, indicating overall decreased conformational heterogeneity. For both ABCA7_{BPL} and
99 ABCA7_{BPE}, greater positional disorder was observed for TMD2-NBD2 compared to TMD1 and
100 NBD1 as indicated by relatively weaker EM density quality (Figure S3).

101 **The ABCA7 TMD lumen is accessible to an ordered file of bilayer lipids**

102 Our ABCA7_{BPL/PE} structures are distinguished from available structures of ABCA1 and
103 ABCA4 (all resolved in a detergent environment) by the wider open TMD lumen that is almost
104 completely occupied by lipids. The observed lipids are continuous with the surrounding membrane
105 except at the cytoplasmic leaflet near residues L655 and T1646 from TM5 and TM11, respectively
106 (Figure 1E-F). EM density for the modeled lipids is recognizable by gaps between the extracellular
107 and cytoplasmic leaflets and the two acyl chains of a single file of phospholipids in the two lipid
108 leaflets. Towards the extracellular end, ECD residues R475, K478, R482, K1407 and TMD1
109 residues R544 and R548 form a cluster of positively charged side chains oriented towards the
110 luminal lipids (Figure 1G). Overall, the luminal lipids are more closely associated with TMD1,
111 with residues from TM2, TM5, and TM11 within 5 Å of the modeled acyl chains compared to only
112 residues from TM11 from TMD2.

113 To compare the architecture of ABCA7 in the presence or absence of lipids, we also
114 determined its structure in the detergent digitonin (Figure 2A-B, Figure S4A-E). This
115 ABCA7_{DIGITONIN} structure revealed a similar overall conformation to that seen in structures of
116 ABCA1²⁶ and ABCA4^{25,27,28} (Figure S4F) with a more complete map for the ECD compared to
117 ABCA7_{BPL/PE}. As expected, no EM density for TMD lipids was visible, and only isolated density
118 features attributable to detergent molecules associated with TMD1 were observed, although only
119 at a contour level below where much of the surrounding detergent micelle was visible (Figure
120 2A,C). This is in contrast to ABCA7_{BPL/PE} structures where TMD lipid density was much stronger
121 than that of the bulk nanodisc (Figure 2D-E), further validating our assignment of bilayer lipids.
122 Compared to structures in nanodiscs, the TMDs in this ABCA7_{DIGITONIN} structure were arranged
123 more symmetrically with respect to each other with a narrower lumen. Interestingly, EM density
124 for TMD2 was still weaker than that of TMD1, in contrast to structures of ABCA4^{25,27,28} and
125 ABCA1²⁶ (Figure S4D) indicating that a more mobile TMD2-NBD2 pair may be a unique feature
126 of ABCA7.

127 **Closed TMD lumen and exit pocket for lipid extrusion in ATP bound ABCA7**

128 To gain insight into possible mechanisms of lipid extrusion from the ABCA7 TMD, we
129 used the hydrolysis-deficient ABCA7_{EQ} mutant reconstituted in BPL/Chol nanodiscs and
130 determined its structure in a closed, ATP-bound state at 3.7 Å resolution (Figure 3A and Figure
131 S5). This ABCA7_{EQ-ATP} structure revealed closely interacting TMD-NBD pairs and a largely
132 occluded TMD lumen (Figure 3B). However, at the extracellular end of the TMD lumen, we
133 observed a small central opening to the extracellular space/ECD that may represent an ‘exit pocket’
134 (Figure 3C,D) akin to that seen in the yeast pleiotropic drug resistance transporter Pdr5²⁹ that could

135 likely accommodate two acyl chains, (Figure 3D). TMD closure involves formation of a 4-TM
136 bundle comprising TMs 2, 5, 8, and 11 that occludes the cytoplasmic bilayer leaflet. The exit
137 pocket is comprised largely of hydrophobic residues, except for R548, which is part of a cluster of
138 positively charged residues including R475, K478, R482 and R678 identified in our ABCA7_{BPL/PE}
139 structures that may aid in directing a negatively charged phospholipid headgroup towards the ECD.
140 Side chain density for this group of basic residues was poor compared to that in ABCA7_{BPL/BPE}
141 structures, indicating greater disorder. TMD closure is accompanied by a rearrangement of both
142 TMD-ECD interfaces compared to the open state structures (Figure S6). Compared to the
143 ABCA7_{BPL} structure, both TMD1 and TMD2 interfaces with ECD1 increased from BSAs of 190
144 Å² to 331 Å² and from 76 Å² to 285 Å², respectively. Conversely, the BSAs of TMD1 and TMD2
145 with ECD2 decreased from 543 Å² to 275 Å² and from 317 Å² to 192 Å², respectively. As
146 expected, the ABCA7_{EQ-ATP} structure shows a canonical NBD sandwich dimer with bound ATP
147 (Figure 3E). In contrast to the ATP bound ABCA4 structure, RD density was too weak for accurate
148 placement. However, contoured at lower thresholds, the available density features were more
149 compatible with a rigid body shift rather than a conformational rearrangement of RD, with RD2
150 appearing to maintain contact with NBD1, but RD1 disengaged from NBD2.

151 **Rigid-body motions of the TMDs define ABCA7 conformational transitions**

152 Despite significant overall conformational differences, the individual TMDs in
153 ABCA7_{BPL/PE}, ABCA7_{DIGITONIN}, and ABCA7_{EQ-ATP} remain largely unaltered (Figure 4A).
154 Moreover, the TMD-NBD pairs move as rigid body units from the fully open ABCA7_{BPL} structure
155 to that of ABCA7_{DIGITONIN}, which we assert is akin to an intermediate open state between the fully
156 open ABCA7_{BPL/PE} state and the closed ABCA7_{EQ-ATP} states. The transition from open to

157 intermediate open involves a rigid-body rotation of 9° and translation of 2 Å for TMD2-NBD2.
158 The transition to the closed state involves a further 6° rotation and 15 Å translation of TMD2-
159 NBD2 (Figure 4B-C), albeit with a greater alteration in the NBDs owing to a movement of their
160 recA like domains upon ATP binding and dimerization. Rigid body movements were also observed
161 for the entire RD in all three structures. The RD of ABCA7_{DIGITONIN} maintained molecular
162 interactions with both NBD1 (RD2) and NBD2 (RD1), whereas the RD of ABCA7_{BPL/PE} separated
163 from NBD2 while maintaining contact with NBD1. Finally, the ECD base region transitioned
164 through a rigid body rotation of 34° and translation of 6.3 Å going from the open to closed states,
165 whereas the tunnel and lid regions displayed greater heterogeneity.

166 To establish whether the concerted TMD-NBD rigid body motions outlined above may
167 extend to other ABC transporters of the Type-V ABC transporter/Type II ABC exporter fold³⁰, we
168 extended our analysis of individual TMD-NBD pairs to members of the G family for which the
169 first structures of open and closed states were available, namely ABCG2 and ABCG5/G8 (Figure
170 S7A)^{31,32}. As shown in Figure S7B, the TMD-NBD pairs from both the apo and ATP-bound closed
171 states of ABCG2, as well as from both halves of ABCG5/G8, all shared a similar overall
172 architecture. Despite the divergent topologies of ABCG and ABCA transporters, with the former
173 are arranged in an NBD-TMD configuration compared to TMD-NBD for the latter, the individual
174 TMD-NBD pairs from ABCA7 shared very strong structural similarities with those of ABCG2,
175 further establishing the role of rigid body movements of the TMDs to affect large scale
176 conformational changes in these transporters.

177 **Lipid partitioning in the ABCA7 TMD captured with MD simulations**

178 To gain additional molecular insight into the TMD-mediated lipid partitioning, membrane
179 perturbation, and lipid extrusion from ABCA7, we performed multi-microsecond MD simulations
180 of the open conformation of ABCA7_{PE} after embedding into two distinct lipid bilayers, one
181 containing PE/Chol (4:1) and the other PC/Chol (4:1) (Figure 5, Figure S8). Each simulation was
182 performed for 2 μ s using a system including four copies of the protein (Figure 5A), resulting in an
183 aggregate 8 μ s sampling of lipid-protein interactions for each lipid composition. Interestingly,
184 during the simulations, we observed PE and PC phospholipids penetrating the TMD cavity in both
185 the cytoplasmic and extracellular leaflets in all four protein replicas (Figure 5A, insets). We
186 quantified the number of phospholipids within the TMD cavity by counting the lipid headgroups
187 (Figure S8C), revealing that on average, ABCA7 accommodated a larger number of PE lipids
188 compared to PC (Figure 5B). To further quantify ABCA7-mediated deformation of the lipid
189 bilayer bridging the TMDs, the average heights of phospholipid headgroups were calculated with
190 respect to the midplane of the bilayer. We captured both a tendency for lipids to move towards the
191 cytoplasmic gate and the formation of a dome-shaped phospholipid arrangement within the TMD
192 lumen (Figure 5C-E, Figure S8A-B). Interestingly, our MD simulations showed an accumulation
193 of phospholipid headgroups in the vicinity of residues R475, K478, R482, R544, and R548, with
194 R482 and R548 displaying the most frequent lipid contacts (Figure S8D-E), corroborating our
195 structural observations. Analysis of the cytoplasmic leaflet highlighted a continuous distribution
196 of phospholipids with the surrounding membrane, except near TM5 and TM11 around residues
197 L655 and T1646 (Figure 5D-E), which correlated well with the bilayer-like density in the
198 ABCA7_{BPL} and ABCA7_{PE} cryo-EM maps (Figure 1C-D) that we modeled with acyl chains.

199 Discussion

200 A mechanistic model derived from our results is shown in Figure 6. We establish that the
201 TMD lumen of ABCA7 is accessible to bilayer lipids in the open state (ABCA7_{BPL/PE}), providing
202 a basis for substrate entry from both the extracellular and cytoplasmic leaflets. These ordered lipids
203 are akin to those observed in the TMD cavity of AcrB, where they have been suggested to be
204 important for functional integrity³³. We identify a network of positively charged residues at the
205 extracellular periphery of TMD1 and the base of the ECD directed towards the TMD luminal
206 lipids. Our MD simulations support a role for these residues in interacting with phospholipid
207 headgroups, consistent with our structural data. In ABCA7, R475 mutations have been identified
208 in AD³⁴ patients, and mutation of R638 in ABCA1 (equivalent to R548 in ABCA7) is associated
209 with reduced serum HDL³⁵ (Figures S9 and S10). While further studies are needed to pinpoint the
210 specific roles, if any of these residues, in ABCA7 function, they remain largely conserved in
211 ABCA1, ABCA4, and ABCA7. The upward protrusion of both bilayer leaflets within the TMD
212 lumen suggested by MD simulations may, upon TMD closure, aid in sequestering phospholipids
213 in the identified exit pocket to be primed for extrusion towards the ECD. Membrane deformations
214 similar to those highlighted here have also been observed in the signal peptidase complex³⁶, and
215 further evidence the influence membrane proteins have on local membrane bilayer structure.
216 ABCA7 could thus play a role in changing its membrane lipid environment by flipping
217 cytoplasmic leaflet lipids to the extracellular leaflet and also extruding them back out into the bulk
218 bilayer environment and/or to apolipoproteins. The reported defects in the phagocytotic activity of
219 cells that express dysfunctional ABCA7^{37,38} could be related to ABCA7's influence on the
220 asymmetric distribution of bilayer lipids³⁹, as enrichment of PS, shown to be flipped by ABCA7¹⁶,
221 at the extracellular surface is linked to phagocytosis and phagocytosis-associated proteins within
222 the membrane⁴⁰⁻⁴².

223 Despite significant progress in our mechanistic understanding of ABCA transporter
224 function, several questions remain open. First, it is unclear to what extent ABCA7 interacts with
225 apolipoproteins in a physiologically relevant manner and, more broadly, the structural basis for
226 apolipoprotein interactions with ABCA7 or ABCA1 is unknown. Second, while our structures
227 provide a potential basis for lipid entry into and extrusion from the ABCA7 TMD, the mechanism
228 whereby lipids get flipped, remains unresolved. Third, while our data point to a potential
229 preference for PE over PC for TMD partitioning, the exact mechanism whereby ABCA1 or
230 ABCA7 achieve lipid specificity are unknown. The observed enhancement in conformational
231 homogeneity, quality of lipid density, and ATPase activity of our ABCA7_{PE} sample may be, in
232 part, due to the smaller PE headgroup, which has been shown to aid in folding and stabilization of
233 membrane proteins⁴³. Finally, it is unknown how the opposite direction of substrate transport for
234 ABCA4 is achieved considering similarities in ATP bound closed and open state structures of
235 ABCA4 and ABCA7. Overall, our data will help devise better *in vitro* and *in silico* models to
236 answer these questions, which will further aid in dissecting the unique roles these proteins play in
237 cellular physiology.

238 **METHODS**

239 **METHODS**

240 **Protein Purification**

241 We utilized the Flp-In TREX system (Thermo Fisher Scientific) for tetracycline inducible
242 expression of human ABCA7. In short, a codon optimized synthetic gene construct
243 (GeneArt/Thermo Fisher Scientific) of isoform 1 of ABCA7 (Uniprot ID Q8IZY2-1), harboring a
244 C-terminal eYFP-Rho1D4 tag⁴³ with a 3C/precision protease site between the protein and

245 purification tags, was cloned into a pCDNA5.1 FRT/TO vector between BamHI and NotI
246 restriction sites and a stable cell line was generated as per manufacturer's protocol (Flp-In™ T-
247 Rex™ Core Kit, Thermo Fisher Scientific). The resulting HEK293 based stable cells were grown
248 and maintained in adherent cell culture in Dulbecco's Modified Eagle Medium (DMEM, Thermo
249 Fisher Scientific) supplemented with 9% Fetal Bovine Serum (FBS, Gibco) and a
250 penicillin/streptomycin mixture (Thermo Fisher Scientific) at 37°C with 5% carbon dioxide (CO₂)
251 under humidified conditions. For protein production, cells were induced with 0.6 µg ml⁻¹
252 tetracycline at a confluency of 80% in fresh DMEM supplemented with 2% FBS under otherwise
253 identical conditions for an additional 72 hours before being washed with Phosphate Buffered
254 Saline (PBS), harvested, and flash frozen in liquid nitrogen.

255 For purification, thawed cells were resuspended in a lysis buffer (Buffer L) comprising 25
256 mM Hepes pH 7.5, 150 mM sodium chloride (NaCl), 20% glycerol, 1 cOmplete EDTA free
257 protease inhibitor tablet (Roche) per 50 ml Buffer L, 800 µM phenylmethylsulfonyl fluoride
258 (PMSF) and 20 µg ml⁻¹ soybean trypsin inhibitor (both Sigma), and mechanically cracked using
259 a dounce homogenizer before addition of a 0.5%/0.1% w:v mixture of dodecyl maltoside (DDM)
260 and cholesteryl hemisuccinate (CHS) (both Anatrace). Protein extraction was allowed to proceed
261 for 90 minutes at 4°C with gentle agitation, after which, the suspension was centrifuged at 48,000
262 r.c.f for 30 minutes and the supernatant applied to rho-1D4 antibody (University of British
263 Columbia) coupled Sepharose resin (Cytiva). Binding was allowed to proceed for 3 hours before
264 the unbound fraction was discarded and beads rinsed with 4 x 10 bed volumes (BVs) of wash
265 buffer (25 mM Hepes pH 7.5, 150 mM NaCl, 20% glycerol, 0.02%/0.004% w:v DDM/CHS).
266 Protein was eluted by incubation with 3 BVs elution buffer (wash buffer supplemented with either
267 3C protease (1:10 w:w 3C:ABCA7) or 0.5 mg ml⁻¹ 1D4 peptide (GenScript)) for 2-18 hours.

268 The EQ variant of ABCA7 contained two site mutations, E965Q and E1951Q. The E965Q
269 site was created within the ABCA7 construct using site directed mutagenesis by PCR with the
270 primers: A7eq1for 5'-GGTCATCCTGGATCAACCTACAGCAGGCGTGG-3' and A7eq1rev
271 5'-GCCTGCTGTAGGTTGATCCAGGATGACCACC-3'. E1951Q was generated using a
272 synthesized dsDNA block and the enzymes NheI and BsiWI. ABCA7_{EQ} with C-terminal eYFP-
273 Rho1D4 tag was then transferred to a pCAG vector using KpnI and NotI restriction sites. The
274 HEK293T cells were grown in Dulbecco's Modified Eagle Medium (DMEM, Scientific)
275 supplemented with 9% FBS (Gibco), penicillin/streptomycin mixture (Scientific) and antimycotic
276 (Gibco) at 37°C and 5% CO₂ under humidified conditions. A mixture of 37.5 µg of ABCA7_{EQ}
277 plasmid and 75 µg of polyethyleneimine (PEI, Sigma) was incubated for 15 min at room
278 temperature before being applied to 15 ml plates of HEK293T cells at a confluency of 60 - 80%
279 to initiate transfection and expression. The cells were further cultured for 72 hours before being
280 washed with PBS, harvested and flash frozen in liquid nitrogen. ABCA7_{EQ} was purified in the
281 same approach of ABCA7; and eluted by incubation with 3 BVs elution buffer with either 3C
282 protease for ATPase assay or with 0.25 mg ml⁻¹ of 1D4 peptide in an additional 2 mM ATP and
283 10 mM MgCl₂ for nanodisc reconstitution.

284 Membrane scaffold protein D1 (MSP1D1, addgene) and apoA1 were purified using
285 established protocols for MSP⁴⁴ with the following modifications: A synthetic construct of apoA1
286 bearing a 3C protease cleavable N-terminal deca-histidine tag (GeneArt/Thermo Fisher Scientific)
287 was cloned into a pET28a vector (Addgene) and transformed in *E. coli* BL21 DE3 cells (New
288 England Biolabs). One-liter cultures of Terrific Broth (TB) supplemented with 50 µg ml⁻¹
289 kanamycin were grown from 10 ml overnight cultures from single colonies grown in LB. Cells
290 were grown to an OD₆₀₀ of 0.8 in a shaking incubator at 37 °C and induced with 1 mM isopropyl

291 β -d-1-thiogalactopyranoside (IPTG). Protein expression was allowed to proceed at 20°C for 12
292 hours. Cells were centrifuged at 12,000 r.c.f, and pellets were flash frozen in liquid nitrogen and
293 stored at -80°C until required. Frozen pellets were resuspended in 8 ml/ gram cell pellet
294 resuspension buffer comprising 25 mM Hepes pH 7.5, 150 mM NaCl and 1 mM
295 phenylmethylsulfonyl fluoride (PMSF) and sonicated. The suspension was spun down at 16,000
296 r.c.f at 4 °C for 30 min and the supernatant was applied 5 ml Ni-NTA resin (Qiagen)/ L culture
297 medium. After discarding the flowthrough, the resin was washed with 25 mM Hepes pH 7.5,
298 150 mM NaCl, 1 mM PMSF and 20 mM imidazole until a pre-established baseline A280 reading
299 was achieved. ApoA1 was eluted in 4 BVs of 25 mM Hepes pH 7.5, 150 mM NaCl, 1 mM PMSF
300 and 200 mM imidazole, concentrated using a 10 kDa molecular weight cutoff (MWCO) Amicon
301 filter (Millipore-Sigma) and desalted using a PD10 column (Cytiva) into 25 mM Hepes pH 7.5,
302 150 mM NaCl. The concentration of apoA1 was adjusted to 1 mg ml⁻¹ for flash freezing in liquid
303 nitrogen and storage at -80°C.

304 **ABCA7 and ABCA7_{EQ} nanodisc and proteoliposome preparation**

305 For nanodisc reconstitution, peptide eluted or 3C cleaved ABCA7 was mixed with
306 MSP1D1 and a mixture of BPL (brain polar lipid extract from Avanti) and cholesterol (80:20 w:w)
307 with 0.5%/0.1% DDM:CHS using a 1:10:350 (ABCA7:MSPD1:lipid mix) molar ratio in nanodisc
308 buffer (25 mM Hepes pH 7.5, 150 mM NaCl) that contained up to 4% glycerol for 30 minutes at
309 room temperature (RT). Nanodisc reconstitution was induced by removing detergent with 0.8 mg
310 ml⁻¹ pre-washed Biobeads SM-2 (Bio-Rad) for 2 hours with gentle agitation at RT. For different
311 phospholipid compositions, BPL was replaced with brain PE, PS, or PS (all from Avanti Polar
312 Lipids). For structural studies, nanodisc-reconstituted ABCA7 bearing the eYFP-Rho1D4 tag was
313 bound to rho-1D4 resin for an additional 2 hours, washed with 4 BV of nanodisc buffer, and eluted

314 with 3C protease for 2 hours at 4°C. The eluted ABCA7 nanodiscs were concentrated using a
315 100,000 MWCO kDa Amicon filter and further purified by size exclusion chromatography using
316 a G4000swxl column (TOSOH biosciences) equilibrated with nanodisc buffer at 4°C. Figure S1A
317 shows a SEC chromatogram for pure ABCA7 placed into BPL/Ch nanodiscs, while a SEC
318 chromatogram for ABCA7 in PE/Ch nanodiscs is in Figure S2A. Generally, three fractions were
319 pooled from the main resultant peak.

320 ABCA7_{EQ} was reconstituted in nanodiscs for cryo-EM preparation using the same
321 approach of ABCA7; except that an additional 2 mM ATP and 10 mM MgCl₂ were present until
322 the end of the purification procedure prior to grid preparation. A SEC chromatogram for ABCA7_{EQ}
323 in BPL/Ch nanodiscs is shown in Figure S5A, where the trace is affected by the additional ATP
324 added during the run.

325 ABCA7 proteoliposomes were generated by mixing detergent purified ABCA7 with
326 liposomes at a protein: liposome ratio of 1:10 w:w. Liposomes were prepared by extruding a 20
327 mg ml⁻¹, 80:20 w:w BPL/Ch lipid mixture 11 times using a previously described protocol ⁴⁵.
328 Briefly, detergent purified ABCA7 and liposomes were added to 0.14% and 0.3% Triton X100
329 (Sigma), respectively, then incubated for 30 minutes at RT. These two samples were mixed and
330 incubated for 60 minutes. Detergent was removed by adding 40 mg fresh Biobeads SM2 (Bio-
331 Rad) per ml reaction mixture during five successive incubation steps, 30 minutes at RT, 60 minutes
332 at 4°C, overnight at 4°C, and two periods of 60 minutes at 4°C with gentle agitation. The
333 suspension was centrifuged at 80,000 rpm for 20 minutes in an ultracentrifuge. The supernatant
334 was removed, and the liposomal pellet was washed once with reconstitution buffer containing 150
335 mM NaCl, 25 mM Hepes pH 7.5. The ABCA7-liposome suspension was then centrifuged to

336 remove the supernatant, and the proteoliposomes were resuspended at a final concentration of
337 0.5 - 1 mg ml⁻¹ for ATPase assays.

338 **ABCA7_{DIGITONIN} preparation**

339 For the digitonin solubilized ABCA7 purification, ABCA7 was extracted from the cell in
340 a lysis buffer (Buffer L) using the same approach above, and the supernatant was applied to rho-
341 1D4 resin for a 3-hour binding period. Then, the resin was rinsed with the 4 x 10 BVs of wash
342 buffer containing 25 mM Hepes pH 7.5, 150 mM NaCl, 20% glycerol (v/v), and 0.06% digitonin
343 (w/v). Protein was eluted by incubation with 3 BVs elution buffer, which was wash buffer
344 supplemented with 3C protease (1:10 w:w 3C:ABCA7). Interestingly we obtained better particle
345 distribution and ice quality with addition of a 1:2.5 molar excess of apoA1, prepared in house, to
346 3C cleaved ABCA7 prior to grid preparation. The mixture was concentrated by a 100,000 MWCO
347 kDa Amicon filter (Millipore) and further purified by size exclusion chromatography using a
348 G4000swxl column (TOSHOH biosciences) equilibrated with a buffer containing 25 mM Hepes
349 pH 7.5, 150 mM NaCl, 0.035% digitonin (w/v), as shown in Figure S4A. Peak fractions were
350 pooled and concentrated for cryo-EM grid preparation.

351 **ATPase assays**

352 ATPase assays were based on a molybdate based colorimetric assay⁴⁶. Protein
353 concentrations used were in the range of 0.05-0.1 mg ml⁻¹. Assays were started by the addition of
354 either 2mM ATP, except for experiments in Figure 1B where 6.25mM ATP was used, in the
355 presence of 10 mM magnesium chloride (MgCl₂), incubated for 30 minutes at 37°C, then stopped
356 by addition of 6% SDS. The assay was also performed in the presence of ABCA7 inhibitors as
357 additives, such as 5 mM ATPγS or sodium orthovanadate. For ATP K_M measurements, a range of
358 ATP concentrations was used. Statistical analysis was done using GraphPad Prism 9. ATPase rates

359 were measured using simple linear regression, and the K_M of detergent, liposome, and nanodisc
360 reconstituted ABCA7 were determined from the fit to the Michaelis-Menten equation of the
361 corresponding rates. ABCA7 concentrations were measured using gel densitometry analyzed in
362 ImageStudio Lite (LI-COR Biosciences) based on detergent purified ABCA7 standards with
363 known concentrations determined by A280 measurements. All reaction components were mixed
364 with ABCA7 in detergent or reconstituted in nanodiscs and liposome in the absence of ATP,
365 incubated for 10 minutes at 37 °C prior to addition of ATP to start the reaction.

366 **Cryo-electron microscopy grid preparation**

367 For ABCA7 reconstituted in nanodisc prepared in 80:20 w:w BPL/cholesterol and
368 PE/cholesterol, SEC purified protein was mixed with 5 mM ATP γ S (TOCRIS) and 5 mM MgCl₂
369 for 20 minutes at room temperature and concentrated to 0.5 - 1.0 mg ml⁻¹. Peak fractions from SEC
370 already containing 2 mM ATP (Sigma) and 10 mM MgCl₂ were pooled and concentrated to 0.5 -
371 1 mg ml⁻¹ for nanodisc reconstituted ABCA7_{EQ-ATP}. For ABCA7 in digitonin, peak fractions were
372 pooled and concentrated between 2 to 5 mg ml⁻¹. 4 μ l samples were applied to glow discharged
373 Quantifoil R1.2/1.3 grids (Electron Microscopy Sciences, Hatfield, PA, USA) using a Vitrobot
374 Mark IV (Thermo Fisher Scientific) with a 4s blotting time and 0 blotting force under >90%
375 humidity at 4°C, then plunge frozen into liquid ethane. For the nanodisc reconstituted ABCA7_{EQ-}
376 _{ATP} and ABCA7 in digitonin, two sample droplets were applied to glow discharged grids to obtain
377 more particles per hole.

378 **Cryo-electron microscopy data collection and processing**

379 Grids were clipped as per manufacturer guidelines and cryo-EM data was collected using
380 a Titan Krios electron microscope operating at 300kV and equipped with a Falcon 3EC direct
381 electron detector (Thermo Fisher Scientific.). Automated data collection was carried out using

382 EPU 2.8.0.1256REL software package (Thermo Fisher Scientific) over multiple sessions in
383 counting mode at a nominal magnification of 96,000x, corresponding to a calibrated pixel size of
384 0.895 Å for nanodisc reconstituted ABCA7_{BPL}. Image stacks comprising 60 frames were collected
385 at a defocus range of -0.6 to -2.6 µm and estimated dose rate of 1 electron/Å²/frame and further
386 processed in Relion-3.1 (beta). Motion correction was done using Motioncor2 (Relion
387 implementation)⁴⁷ and contrast transfer function (CTF) correction was performed using Gctf 1.06
388 ⁴⁸. A summary of the overall data processing scheme and the quality was presented in Figure S1C-
389 E. In brief, 11802 micrographs were used for template free picking of 6725108 particles, followed
390 by particle extraction at a 3x binned pixel size of 2.685 Å/pix. The dataset was processed in two
391 batches. After 2-3 rounds of 2D classification 1259324 particles from Set 1 and 1088487 particles
392 from Set 2 were selected for independent 3D classification steps (number of classes (K)=8 for
393 both). The structure of human ABCA1 (EMDB6724) was used as a 3D reference for an initial 3D
394 classification of a subset of the total data to yield an initial sub-nanometer resolution map of
395 ABCA7 that was used as a 3D reference for the full datasets. After 1 round of 3D classification,
396 both sets of data yielded a similar ensemble of classes. A total of 113291 particles from similar
397 looking classes (black boxes) were subjected to an additional round of classification (K=3), ~80%
398 of which fell into a high-resolution class that yielded a 3.6 Å map after refinement and particle
399 polishing steps. Similarly, 124114 particles from a second set of two similar classes (red boxes in
400 Figure S1D) were selected for subsequent refinement, particle polishing, and post processing to
401 yield a 3.1 Å map. All resolution estimates were based on the gold standard 0.143 cutoff criterion
402 ⁴⁹. Datasets of ABCA7_{PE}, ABCA7_{EQ-ATP}, and ABCA7_{DIGITONIN} were collected at a nominal
403 magnification of 96,000x corresponding to a calibrated pixel size 0.889 Å, and image stacks
404 containing 40 frames were collected a defocus range of -0.8 to -2.6 µm with an estimated dose rate

405 of 1 electron/Å²/frame and further processed using the same software versions as for the
406 ABCA7_{BPL} dataset unless otherwise indicated.

407 For ABCA7_{PE}, a total of 2849251 particles were picked from 9218 ctf corrected (Gctf)
408 micrographs in Relion ver. 3.1 in two batches at a 3-fold binned pixel size of 2.667 Å/pixel (Figure
409 S2B-D). Of these, 783655 particles and 413330 particles were selected from Batch 1 and Batch
410 2, respectively and independently subjected to 3D classification (K=8) using a low pass filtered
411 (60 Å) map of our ABCA7_{BPL} structure as a reference. A single highest resolution class from each
412 was selected and their particles combined and subjected to an additional round of 2D classification.
413 2024649 particles were subjected to another round of 3D classification (K=8). A single, highest
414 resolution class containing 50704 particles was refined to 5.4 Å. Particles were re-extracted using
415 refined coordinates and unbinned (pixel size 0.889 Å/pixel) and subjected to a round of 3D
416 refinement, Bayesian Polishing, and postprocessing/B-factor sharpening to yield a final map 4.0
417 Å resolution and its local resolution filtered variant calculated using Relion's own algorithm. Local
418 resolution maps are shown for ABCA7_{BPL} (Map1 & Map2) and ABCA7_{PE} in Figure S3.

419 For the ABCA7_{DIGITONIN} dataset (Figure S4B-E), a total of 7437149 particles were picked
420 from 16213 ctf corrected and motion corrected micrographs and extracted at a 3-fold binned pixel
421 size of 2.667 Å/ pixel. After 2D classification, 1220497 particles were subjected to 3D
422 classification (K=8) using a low pass filtered (60 Å) map of our ABCA7_{BPL} structure as a reference.
423 A single class comprising 324727 particles was refined to 5.4 Å. The refined coordinates were
424 then used to re-extract unbinned particles (0.889 Å/pixel), subjected to 3D refinement, and
425 Bayesian polishing. Further 3D classification (K=5) was performed and two similar classes
426 containing 149590 particles were picked for 3D refinement and postprocessing/B-factor
427 Sharpening to yield a 3.9 Å map.

428 For the ABCA7_{EQ-ATP} dataset, an initial set of 2660267 particles were picked from 4914
429 ctf corrected micrographs (Figure S5B-E). After 2D classification, 469397 particles were subjected
430 to initial model building. This model was used as a 3D reference to perform 3D classification
431 (k=5). A single class comprising 174415 particles was refined to 5.4 Å, the corresponding particles
432 unbinned and re-refined. The nanodisc density was subtracted within Relion, followed by 3D
433 classification (k=3). The highest resolution class comprising 51780 particles was refined to 4.3
434 Angstroms and used for 3D reference-based particle picking for a larger data set comprising the
435 initial 4914 movies and a new set of 4474 ctf corrected micrographs. A total of 3773280 particles
436 were picked and subjected to multiple rounds of 2D classification in Relion 4.0-beta. 898916
437 particles were subjected to 3D classification (K=3) and a single highest resolution class consisting
438 of 407424 particles was refined to 5.4 Å. The refined coordinates were then used to re-extract the
439 respective particles without binning (0.889 Å/ pixel) and refined again before 3D classification
440 (K=5). A single class comprising 177230 particles was selected and subjected to 3D refinement,
441 Bayesian polishing, and postprocessing/B-factor sharpening to yield a final map at 3.7 Å.

442 **Model building and refinement**

443 Model building was done in coot 0.9.5⁵⁰ using a combination of Map 1 and its local
444 resolution filtered variant and Map 2. Both Map 1 and Map 2 displayed significant conformational
445 heterogeneity in the second half of ABCA7, with the quality of density in Map 1 allowing
446 placement of a TMD2 model guided in part by the homologous ABCA1 structure. Density
447 attributed to inter-TMD phospholipids was clearest in Map 1. Map 2 revealed very poor and
448 discontinuous density for TMD2-NBD2 but significantly better density for TMD1-NBD1 and the
449 majority of ECD1 and ECD2, allowing for de novo model building. The model for ECD was also
450 guided by the presence of nine glycosylation sites (N78, N98, N312, N340, N1335, N1381, N1386,

451 N1457, & N1518) as well as 4 disulfide bond pairs. Density for the lid region of the ECD was
452 missing in both maps. Model building for both NBDs was guided by structures of the homologous
453 transporters TM287⁵¹, ABCG2, and ABCA1, where density features did not allow for de novo
454 model building. We observed extra density at the nucleotide binding sites for both NBDs despite
455 their open conformation. The structure of the RD was based on a homology model of the predicted
456 RD structure in ABCA4²⁵. The quality of density for the ABCA7 RD allowed rigid body placement
457 for the entire domain. Restrained real space refinement of the model was carried out in Phenix
458 1.19.1⁵² using automatically generated secondary structure restraints. Structural figures were
459 prepared in UCSF Chimera v. 1.13.1⁵³, ChimeraX v. 1.2.5⁵⁴, and PyMOL 2.4.1 (The PyMOL
460 Molecular Graphics System, Version 1.8 Schrödinger, LLC).

461 The model for ABCA7_{PE} was generated by rigid body placement of the ABCA7_{BPL} model
462 followed by real space refinement in phenix as described above. The model for ABCA7_{DIGITONIN}
463 was generated by rigid body fitting each TMD, NBD, ECD, and RD into its postprocessed map
464 followed by manual adjustment of sidechains as allowed for the map. Non proteinaceous EM
465 density was modeled as a CHS and Digitonin (ligand ID Y01) molecule. The corrected model was
466 real space refined against the postprocessed map. The model for ABCA7_{EQ-ATP} was built starting
467 with a homology model based on the ATP bound structure of ABCA4 (PDB 7LKZ), followed by
468 manual adjustment of the structure as required and permitted by the map. The ECD was replaced
469 by a rigid body fitted model of the ECD from the ABAC7_{Digitonin} structure. This model was then
470 refined against both the postprocessed map, and its local resolution filtered counterpart.

471 **MD simulations**

472 We employed MD simulations to capture the arrangement and dynamics of the lipid bilayer
473 induced by the experimentally derived open conformation of ABCA7_{PE}, which was used as the

474 starting model in all the simulations. For system setup, a C-terminal carboxylate capping group,
475 an N-terminal ammonium capping group and all the hydrogen atoms were added using the PSFGEN
476 plugin of VMD (Visual Molecular Dynamics)⁵⁶. The resulting all-atom (AA) model was then
477 converted to a coarse-grained (CG) Martini model using the MARTINIZE protocol
478 (<http://www.cgmartini.nl/>), using an elastic network on atom pairs within a 10-Å cutoff. The
479 Orientations of Proteins in Membranes (OPM) database⁵⁷ was used to identify and align the
480 transmembrane region of the protein with the membrane normal. The protein was embedded in
481 two distinct lipid bilayers (palmitoyl-oleoyl-phosphatidyl-ethanolamine (POPE) and cholesterol
482 with a molar ratio of 4:1 (POPE/Chol), and palmitoyl-oleoyl-phosphatidyl-choline (POPC) and
483 cholesterol with a molar ratio of 4:1 (POPC/Chol), respectively). The protein secondary structure
484 was defined from the AA model and was maintained throughout the CG simulations by the applied
485 elastic network. To increase the sampling of lipid-protein interactions and improve statistics, four
486 independent copies of the CG protein were placed at a distance of 200 Å in a large lipid bilayer
487 (400×400 Å²). The system was then solvated and ionized with 150 mM salt using INSANE⁵⁸.

488 The systems were simulated employing GROMACS 2021.3^{59,60}. A 20-fs timestep was
489 employed in all the simulations. The temperature was maintained at 310 K with a velocity-
490 rescaling thermostat⁶¹ employing a coupling time constant of 1 ps. A semi-isotropic 1 bar pressure
491 was maintained using the Berendsen barostat⁶² with a compressibility and relaxation time constant
492 of 3×10⁻⁴ bar and 5 ps, respectively. The systems were energy minimized for 1,000 steps, followed
493 by short equilibration runs of 18 ns, while restraints were applied to lipid bilayer headgroups and
494 protein backbones. During this time the restraints on bilayer headgroups were reduced gradually
495 from $k = 200 \text{ kJ.mol}^{-1}.\text{nm}^{-2}$ to zero, whereas the protein backbones' restraints ($k = 1,000 \text{ kJ.mol}^{-1}.\text{nm}^{-2}$)
496 were kept constant. Each system was then simulated for 2 μs, with restraints only applied

497 to the protein backbones, resulting in an aggregate sampling of 8 μs (4 copies \times 2 μs). All the
498 systems were simulated following the same MD protocol.

499 All the molecular images were generated using VMD⁵⁶. The membrane deformation
500 induced by ABCA7 was quantified by calculating the z distance of the lipid phosphate moieties
501 (PO_4 bead type in MARTINI) with respect to the bilayer midplane, over the last 1 μs of each
502 trajectory. The generated histogram (binned in $2 \times 2 \text{ \AA}^2$ bins) in each leaflet illustrates the spatial
503 distribution of the height of the lipid head groups within each leaflet. We quantified the differential
504 movement of POPE and POPC within the protein lumen by calculating the number of
505 phospholipids located within the TMDs. If the PO_4 bead of a phospholipid was within 22.5 \AA and
506 12.5 \AA in x and y , respectively, with respect to a protein's center in the x - y plane (membrane plane),
507 then the phospholipid was considered to be within the TMD lumen (Figure S9C).

508 **Acknowledgments**

509 We would like to thank Dr. Kaspar Locher at ETH, Zurich, Switzerland, for providing the
510 synthetic gene construct of ABCA7. We would also like to thank the cryo-EM and shared
511 instruments core facilities at the Hormel Institute for help with experimental setup, and Dr.
512 Rhoderick Brown, Dr. Jarrod French and Dr. Jeppe Olsen for critical reading and discussion during
513 manuscript preparation. This work was supported in part by the Hormel Foundation (Institutional
514 research funds to AA), the National Institutes of Health (NIH) award 1R21-AG069180-01A1 (to
515 AA), and the Cure Alzheimer's fund (to TK). The computational component of the project was
516 supported by the NIH awards P41-GM104601 (to ET) and R01-GM123455 (to ET). We also
517 acknowledge computing resources provided by Blue Waters at National Center for
518 Supercomputing Applications (NCSA), and by eXtreme Science and Engineering Discovery
519 Environment (XSEDE) (grant MCA06N060 to ET), and by Microsoft Azure.

520 Author Contributions

521 AA conceived the research. LTML, JRT, and AA performed all experiments. MD simulations
522 were conducted and analyzed by SD, SP, and ET. TK participated in assay design. LTML, JRT,
523 and AA wrote the manuscript with input from all other authors.

524 Declaration of Interests

525 SP is currently an employee of Loxo Oncology @ Lilly and is a shareholder of stock in Eli Lilly
526 and Co. The rest of the authors declare no competing interests.

527 Data and materials availability:

528 The cryo-EM Maps have been deposited at the Electron Microscopy Databank (EMDB) under
529 accession codes EMD-AAAAA (ABCA7_{BPL} Map 1), EMD-BBBBB (ABCA7_{BPL} Map 2), EMD-
530 CCCCC (ABCA7_{PE}), EMD-DDDDD (ABCA7_{EQ-ATP}), and EMD-EEEEEE (ABCA7_{DI_{GITONIN}}). The
531 associated atomic coordinates have been deposited at the Protein Data bank (PDB) under accession
532 codes 1WWW (ABCA7_{BPL}), 2XXX(ABCA7_{PE}), 3YYY, (ABCA7_{EQ-ATP}), and 4ZZZ
533 (ABCA7_{DI_{GITONIN}}).

534 References

- 535 1 Albrecht, C. & Viturro, E. The ABCA subfamily--gene and protein structures, functions
536 and associated hereditary diseases. *Pflugers Arch* **453**, 581-589, doi:10.1007/s00424-006-
537 0047-8 (2007).
- 538 2 Brooks-Wilson, A. *et al.* Mutations in ABC1 in Tangier disease and familial high-density
539 lipoprotein deficiency. *Nat Genet* **22**, 336-345, doi:10.1038/11905 (1999).
- 540 3 Allikmets, R. *et al.* Mutation of the Stargardt disease gene (ABCR) in age-related
541 macular degeneration. *Science* **277**, 1805-1807, doi:10.1126/science.277.5333.1805
542 (1997).
- 543 4 Akiyama, M. *et al.* Mutations in lipid transporter ABCA12 in harlequin ichthyosis and
544 functional recovery by corrective gene transfer. *J Clin Invest* **115**, 1777-1784,
545 doi:10.1172/JCI24834 (2005).
- 546 5 Hollingworth, P. *et al.* Common variants at ABCA7, MS4A6A/MS4A4E, EPHA1, CD33
547 and CD2AP are associated with Alzheimer's disease. *Nat Genet* **43**, 429-435,
548 doi:10.1038/ng.803 (2011).

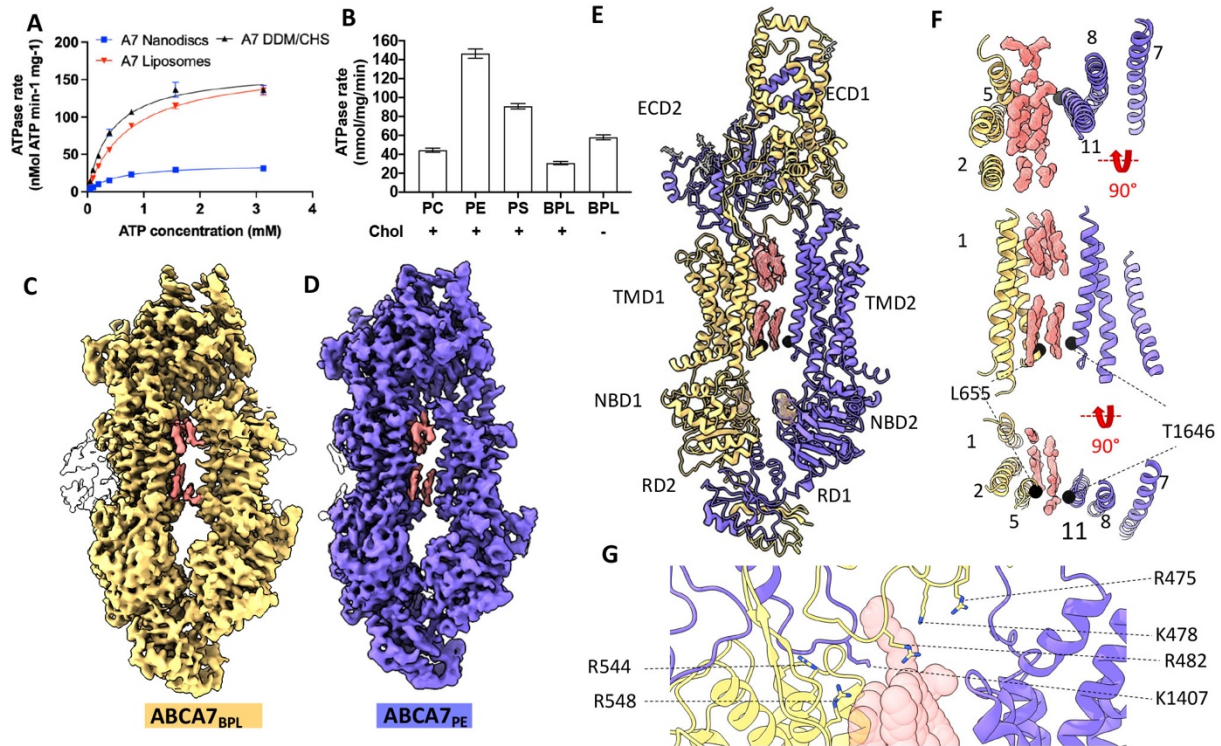
- 549 6 Almeida, J. F. F., Dos Santos, L. R., Trancozo, M. & de Paula, F. Updated Meta-Analysis
550 of BIN1, CR1, MS4A6A, CLU, and ABCA7 Variants in Alzheimer's Disease. *J Mol*
551 *Neurosci* **64**, 471-477, doi:10.1007/s12031-018-1045-y (2018).
- 552 7 Bellenguez, C. *et al.* Contribution to Alzheimer's disease risk of rare variants in TREM2,
553 SORL1, and ABCA7 in 1779 cases and 1273 controls. *Neurobiol Aging* **59**, 220 e221-
554 220 e229, doi:10.1016/j.neurobiolaging.2017.07.001 (2017).
- 555 8 Le Guennec, K. *et al.* ABCA7 rare variants and Alzheimer disease risk. *Neurology* **86**,
556 2134-2137, doi:10.1212/WNL.0000000000002627 (2016).
- 557 9 Swerdlow, R. H. Rare ABCA7 variants in Alzheimer disease: Guilt by association.
558 *Neurology* **86**, 2118-2119, doi:10.1212/WNL.0000000000002630 (2016).
- 559 10 Lambert, J. C. *et al.* Meta-analysis of 74,046 individuals identifies 11 new susceptibility
560 loci for Alzheimer's disease. *Nat Genet* **45**, 1452-1458, doi:10.1038/ng.2802 (2013).
- 561 11 Ma, F. C. *et al.* Meta-Analysis of the Association between Variants in ABCA7 and
562 Alzheimer's Disease. *J Alzheimers Dis* **63**, 1261-1267, doi:10.3233/JAD-180107 (2018).
- 563 12 De Roeck, A., Van Broeckhoven, C. & Sleegers, K. The role of ABCA7 in Alzheimer's
564 disease: evidence from genomics, transcriptomics and methylomics. *Acta Neuropathol*
565 **138**, 201-220, doi:10.1007/s00401-019-01994-1 (2019).
- 566 13 Aikawa, T. *et al.* ABCA7 Regulates Brain Fatty Acid Metabolism During LPS-Induced
567 Acute Inflammation. *Front Neurosci* **15**, 647974, doi:10.3389/fnins.2021.647974 (2021).
- 568 14 Serhan, C. N. Pro-resolving lipid mediators are leads for resolution physiology. *Nature*
569 **510**, 92-101, doi:10.1038/nature13479 (2014).
- 570 15 Astudillo, A. M., Balboa, M. A. & Balsinde, J. Selectivity of phospholipid hydrolysis by
571 phospholipase A2 enzymes in activated cells leading to polyunsaturated fatty acid
572 mobilization. *Biochim Biophys Acta Mol Cell Biol Lipids* **1864**, 772-783,
573 doi:10.1016/j.bbalip.2018.07.002 (2019).
- 574 16 Quazi, F. & Molday, R. S. Differential phospholipid substrates and directional transport
575 by ATP-binding cassette proteins ABCA1, ABCA7, and ABCA4 and disease-causing
576 mutants. *J Biol Chem* **288**, 34414-34426, doi:10.1074/jbc.M113.508812 (2013).
- 577 17 Tomioka, M. *et al.* Lysophosphatidylcholine export by human ABCA7. *Biochim Biophys*
578 *Acta Mol Cell Biol Lipids* **1862**, 658-665, doi:10.1016/j.bbalip.2017.03.012 (2017).
- 579 18 Tonnes, E. & Trushina, E. Oxidative Stress, Synaptic Dysfunction, and Alzheimer's
580 Disease. *J Alzheimers Dis* **57**, 1105-1121, doi:10.3233/JAD-161088 (2017).
- 581 19 Newcombe, E. A. *et al.* Inflammation: the link between comorbidities, genetics, and
582 Alzheimer's disease. *J Neuroinflammation* **15**, 276, doi:10.1186/s12974-018-1313-3
583 (2018).
- 584 20 Czubowicz, K., Jesko, H., Wencel, P., Lukiw, W. J. & Strosznajder, R. P. The Role of
585 Ceramide and Sphingosine-1-Phosphate in Alzheimer's Disease and Other
586 Neurodegenerative Disorders. *Mol Neurobiol* **56**, 5436-5455, doi:10.1007/s12035-018-
587 1448-3 (2019).
- 588 21 Testa, G. *et al.* Changes in brain oxysterols at different stages of Alzheimer's disease:
589 Their involvement in neuroinflammation. *Redox Biol* **10**, 24-33,
590 doi:10.1016/j.redox.2016.09.001 (2016).
- 591 22 Popp, J. *et al.* Cholesterol metabolism is associated with soluble amyloid precursor
592 protein production in Alzheimer's disease. *J Neurochem* **123**, 310-316,
593 doi:10.1111/j.1471-4159.2012.07893.x (2012).

- 594 23 Slegers, K. Expression of ABCA7 in Alzheimer's disease. *Acta Neuropathol* **139**, 941-
595 942, doi:10.1007/s00401-020-02136-8 (2020).
- 596 24 Iwamoto, N., Abe-Dohmae, S., Sato, R. & Yokoyama, S. ABCA7 expression is regulated
597 by cellular cholesterol through the SREBP2 pathway and associated with phagocytosis. *J*
598 *Lipid Res* **47**, 1915-1927, doi:10.1194/jlr.M600127-JLR200 (2006).
- 599 25 Liu, F., Lee, J. & Chen, J. Molecular structures of the eukaryotic retinal importer
600 ABCA4. *Elife* **10**, doi:10.7554/eLife.63524 (2021).
- 601 26 Qian, H. *et al.* Structure of the Human Lipid Exporter ABCA1. *Cell* **169**, 1228-1239
602 e1210, doi:10.1016/j.cell.2017.05.020 (2017).
- 603 27 Scortecci, J. F. *et al.* Cryo-EM structures of the ABCA4 importer reveal mechanisms
604 underlying substrate binding and Stargardt disease. *Nat Commun* **12**, 5902,
605 doi:10.1038/s41467-021-26161-7 (2021).
- 606 28 Xie, T., Zhang, Z., Fang, Q., Du, B. & Gong, X. Structural basis of substrate recognition
607 and translocation by human ABCA4. *Nat Commun* **12**, 3853, doi:10.1038/s41467-021-
608 24194-6 (2021).
- 609 29 Harris, A. *et al.* Structure and efflux mechanism of the yeast pleiotropic drug resistance
610 transporter Pdr5. *Nat Commun* **12**, 5254, doi:10.1038/s41467-021-25574-8 (2021).
- 611 30 Thomas, C. *et al.* Structural and functional diversity calls for a new classification of ABC
612 transporters. *FEBS Lett* **594**, 3767-3775, doi:10.1002/1873-3468.13935 (2020).
- 613 31 Orlando, B. J. & Liao, M. ABCG2 transports anticancer drugs via a closed-to-open
614 switch. *Nat Commun* **11**, 2264, doi:10.1038/s41467-020-16155-2 (2020).
- 615 32 Manolaridis, I. *et al.* Cryo-EM structures of a human ABCG2 mutant trapped in ATP-
616 bound and substrate-bound states. *Nature* **563**, 426-430, doi:10.1038/s41586-018-0680-3
617 (2018).
- 618 33 Qiu, W. *et al.* Structure and activity of lipid bilayer within a membrane-protein
619 transporter. *Proc Natl Acad Sci U S A* **115**, 12985-12990, doi:10.1073/pnas.1812526115
620 (2018).
- 621 34 Cuyvers, E. *et al.* Mutations in ABCA7 in a Belgian cohort of Alzheimer's disease
622 patients: a targeted resequencing study. *Lancet Neurol* **14**, 814-822, doi:10.1016/S1474-
623 4422(15)00133-7 (2015).
- 624 35 Cohen, J. C. *et al.* Multiple rare alleles contribute to low plasma levels of HDL
625 cholesterol. *Science* **305**, 869-872, doi:10.1126/science.1099870 (2004).
- 626 36 Liaci, A. M. *et al.* Structure of the human signal peptidase complex reveals the
627 determinants for signal peptide cleavage. *Mol Cell* **81**, 3934-3948 e3911,
628 doi:10.1016/j.molcel.2021.07.031 (2021).
- 629 37 Tanaka, N., Abe-Dohmae, S., Iwamoto, N., Fitzgerald, M. L. & Yokoyama, S. Helical
630 apolipoproteins of high-density lipoprotein enhance phagocytosis by stabilizing ATP-
631 binding cassette transporter A7. *J Lipid Res* **51**, 2591-2599, doi:10.1194/jlr.M006049
632 (2010).
- 633 38 Abe-Dohmae, S. Y., S. . ABCA7: a potential mediator between cholesterol homeostasis
634 and the host defense system. *Clinical Lipidology* **7**, 677-687 (2012).
- 635 39 Zachowski, A. Phospholipids in animal eukaryotic membranes: transverse asymmetry
636 and movement. *Biochem J* **294** (Pt 1), 1-14, doi:10.1042/bj2940001 (1993).
- 637 40 Gabande-Rodriguez, E., Keane, L. & Capasso, M. Microglial phagocytosis in aging and
638 Alzheimer's disease. *J Neurosci Res* **98**, 284-298, doi:10.1002/jnr.24419 (2020).

- 639 41 Hirt, U. A. & Leist, M. Rapid, noninflammatory and PS-dependent phagocytic clearance
640 of necrotic cells. *Cell Death Differ* **10**, 1156-1164, doi:10.1038/sj.cdd.4401286 (2003).
- 641 42 Fadok, V. A., de Cathelineau, A., Daleke, D. L., Henson, P. M. & Bratton, D. L. Loss of
642 phospholipid asymmetry and surface exposure of phosphatidylserine is required for
643 phagocytosis of apoptotic cells by macrophages and fibroblasts. *J Biol Chem* **276**, 1071-
644 1077, doi:10.1074/jbc.M003649200 (2001).
- 645 43 Raja, M. Do small headgroups of phosphatidylethanolamine and phosphatidic acid lead
646 to a similar folding pattern of the K(+) channel? *J Membr Biol* **242**, 137-143,
647 doi:10.1007/s00232-011-9384-4 (2011).
- 648 44 Molday, L. L. & Molday, R. S. 1D4: a versatile epitope tag for the purification and
649 characterization of expressed membrane and soluble proteins. *Methods Mol Biol* **1177**, 1-
650 15, doi:10.1007/978-1-4939-1034-2_1 (2014).
- 651 45 Ritchie, T. K. *et al.* Chapter 11 - Reconstitution of membrane proteins in phospholipid
652 bilayer nanodiscs. *Methods Enzymol* **464**, 211-231, doi:10.1016/S0076-6879(09)64011-8
653 (2009).
- 654 46 Geertsma, E. R., Nik Mahmood, N. A., Schuurman-Wolters, G. K. & Poolman, B.
655 Membrane reconstitution of ABC transporters and assays of translocator function. *Nat*
656 *Protoc* **3**, 256-266, doi:10.1038/nprot.2007.519 (2008).
- 657 47 Chifflet, S., Torriglia, A., Chiesa, R. & Tolosa, S. A method for the determination of
658 inorganic phosphate in the presence of labile organic phosphate and high concentrations
659 of protein: application to lens ATPases. *Anal Biochem* **168**, 1-4 (1988).
- 660 48 Zheng, S. Q. *et al.* MotionCor2: anisotropic correction of beam-induced motion for
661 improved cryo-electron microscopy. *Nat Methods* **14**, 331-332, doi:10.1038/nmeth.4193
662 (2017).
- 663 49 Zhang, K. Gctf: Real-time CTF determination and correction. *J Struct Biol* **193**, 1-12,
664 doi:10.1016/j.jsb.2015.11.003 (2016).
- 665 50 Scheres, S. H. & Chen, S. Prevention of overfitting in cryo-EM structure determination.
666 *Nat Methods* **9**, 853-854, doi:10.1038/nmeth.2115 (2012).
- 667 51 Emsley, P., Lohkamp, B., Scott, W. G. & Cowtan, K. Features and development of Coot.
668 *Acta Crystallogr D Biol Crystallogr* **66**, 486-501, doi:10.1107/S0907444910007493
669 (2010).
- 670 52 Hohl, M., Briand, C., Grutter, M. G. & Seeger, M. A. Crystal structure of a heterodimeric
671 ABC transporter in its inward-facing conformation. *Nat Struct Mol Biol* **19**, 395-402,
672 doi:10.1038/nsmb.2267 (2012).
- 673 53 Adams, P. D. *et al.* PHENIX: a comprehensive Python-based system for macromolecular
674 structure solution. *Acta Crystallogr D Biol Crystallogr* **66**, 213-221,
675 doi:10.1107/S0907444909052925 (2010).
- 676 54 Pettersen, E. F. *et al.* UCSF Chimera--a visualization system for exploratory research and
677 analysis. *J Comput Chem* **25**, 1605-1612, doi:10.1002/jcc.20084 (2004).
- 678 55 Pettersen, E. F. *et al.* UCSF ChimeraX: Structure visualization for researchers, educators,
679 and developers. *Protein Sci* **30**, 70-82, doi:10.1002/pro.3943 (2021).
- 680 56 Humphrey, W., Dalke, A. & Schulten, K. VMD: visual molecular dynamics. *J Mol*
681 *Graph* **14**, 33-38, 27-38, doi:10.1016/0263-7855(96)00018-5 (1996).
- 682 57 Lomize, M. A., Lomize, A. L., Pogozheva, I. D. & Mosberg, H. I. OPM: orientations of
683 proteins in membranes database. *Bioinformatics* **22**, 623-625,
684 doi:10.1093/bioinformatics/btk023 (2006).

685 58 Wassenaar, T. A., Ingolfsson, H. I., Bockmann, R. A., Tieleman, D. P. & Marrink, S. J.
686 Computational Lipidomics with insane: A Versatile Tool for Generating Custom
687 Membranes for Molecular Simulations. *J Chem Theory Comput* **11**, 2144-2155,
688 doi:10.1021/acs.jctc.5b00209 (2015).
689 59 Hess, B., Kutzner, C., van der Spoel, D. & Lindahl, E. GROMACS 4: Algorithms for
690 Highly Efficient, Load-Balanced, and Scalable Molecular Simulation. *J Chem Theory*
691 *Comput* **4**, 435-447, doi:10.1021/ct700301q (2008).
692 60 de Jong, D. H. *et al.* Improved Parameters for the Martini Coarse-Grained Protein Force
693 Field. *J Chem Theory Comput* **9**, 687-697, doi:10.1021/ct300646g (2013).
694 61 Bussi, G., Donadio, D. & Parrinello, M. Canonical sampling through velocity rescaling. *J*
695 *Chem Phys* **126**, 014101, doi:10.1063/1.2408420 (2007).
696 62 H. J. C. Berendsen, J. P. M. P., W. F. van Gunsteren, A. DiNola, and J. R. Haak.
697 Molecular dynamics with coupling to an external bath. *J. Chem. Phys.* **91**,
698 doi:10.1063/1.448118 (1984).
699
700

701 **Figures and Legends**



702

703 **Figure 1. Functional characterization and structure of human ABCA7 incorporated in**
 704 **nanodiscs (A)** ATPase activity of ABCA7 at different ATP concentrations and **(B)** different
 705 nanodisc phospholipid/cholesterol compositions. Cholesterol (20%) presence is indicated by + or
 706 -. Experimental replicates (n)=3 and error bars represent standard deviation (s.d). **(C)** Cryo-EM
 707 map of ABCA7_{BPL} (yellow) at 3.6 Å resolution and **(D)** ABCA7_{PE} at 4.0 Å resolution (purple).
 708 Density for protein is shown in yellow (0.025 contour) and that for modeled lipid acyl chains
 709 (0.035 contour) shown in pink (TMD luminal lipids) and white (peripherally associated lipids).
 710 **(E)** ABCA7_{PE} shown in ribbon format with Half 1 colored yellow and Half 2 purple, along with
 711 density for TMD lipids (pink 0.025 contour) and bound nucleotide (yellow 0.035 contour). Acyl
 712 chains and glycans are shown as pink and grey sticks, respectively. **(F)** TMD lumen with density
 713 for TMD lipids (pink 0.025 contour) viewed from the extracellular side (top), membrane plane
 714 (middle) and cytoplasmic side (bottom). Ca atoms for the cytoplasmic gate are shown as black
 715 spheres. **(G)** View of the TMD-ECD interface with select residues oriented towards lipids
 716 (transparent red spheres) shown.

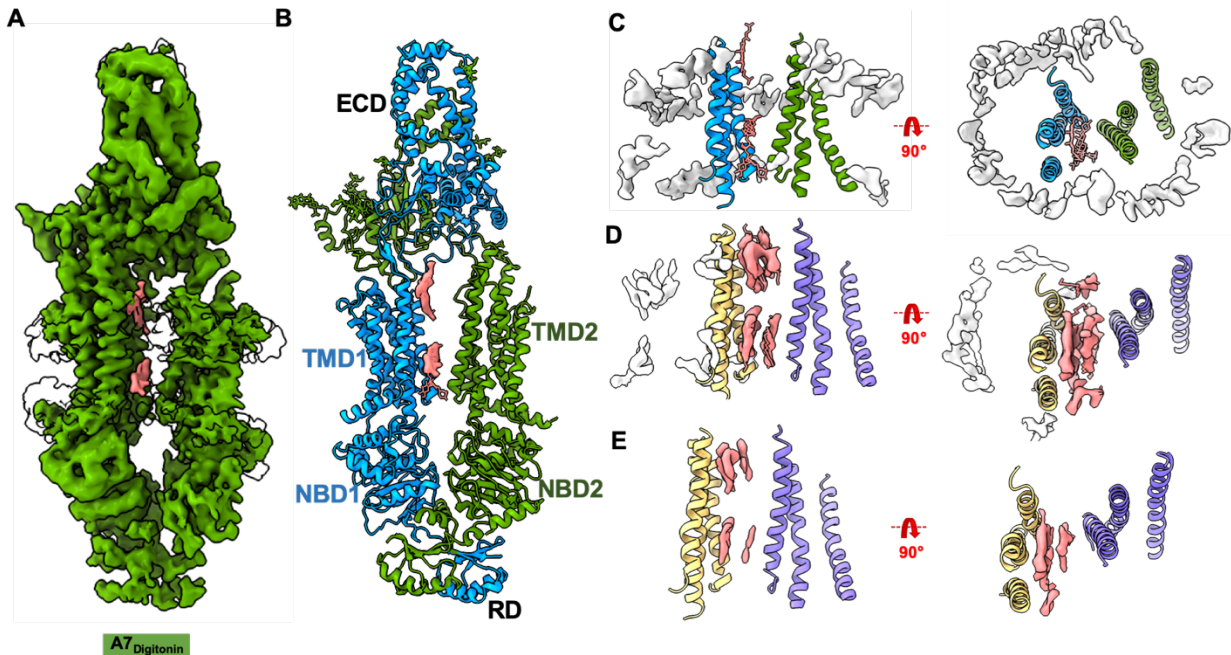
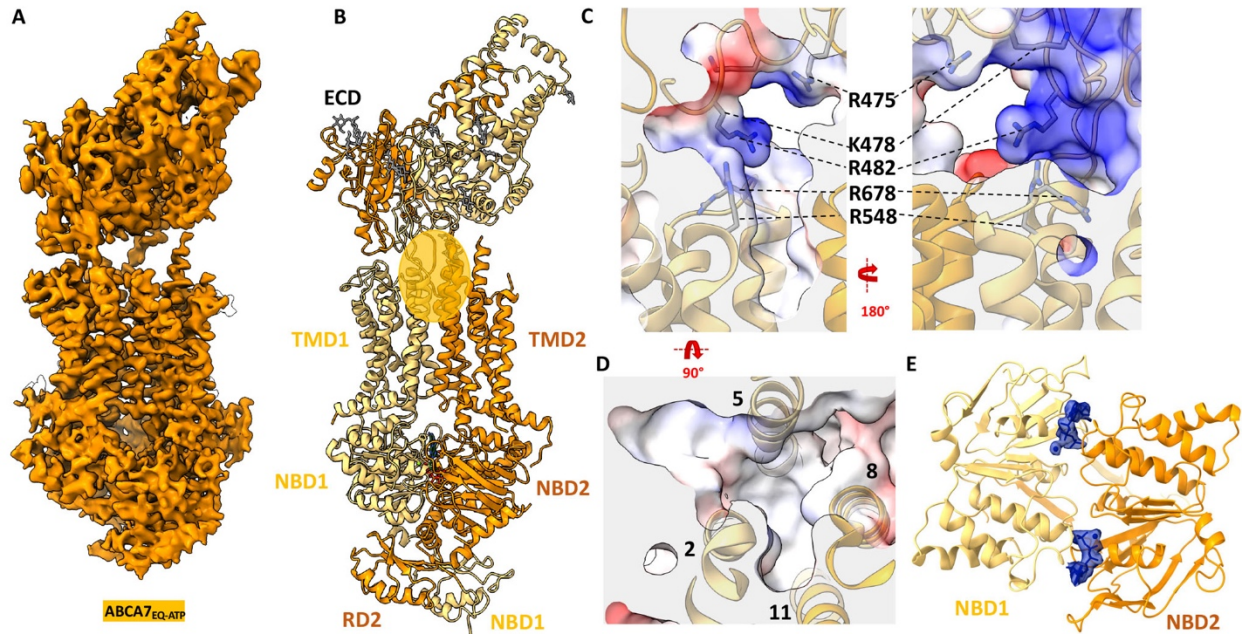


Figure 2. Cryo-EM structure of ABCA7_{DIGITONIN}. (A) Cryo-EM map of human ABCA7_{DIGITONIN} at 3.9 Å with density for protein shown in green (0.013 contour) and extraneous density likely belonging to detergent shown in pink (0.013 contour). (B) Cryo-EM structure of human ABCA7_{DIGITONIN} shown in ribbon format with each half colored differently (blue and green). (C) TMD lumen of ABCA7_{DIGITONIN} with density for bulk micelle shown in white at 0.015 contour where detergent density inside TMDs disappears. Sticks for unmodeled detergent molecules are shown for which density is visible at the lower contour of 0.013. (D) TMD lumen of ABCA7_{PE} with density (0.035 contour) for TMD lipids (pink) and peripherally associated ordered lipids (white) shown. (E) Same as D with higher density contour of 0.046 where density of peripherally associated lipids is absent but that of luminal lipids remains.



729

730 **Figure 3. Cryo-EM structure of ABCA7_{EQ-ATP}.** (A) Cryo-EM map of human ABCA7_{EQ-ATP} in

731 BPL/Chol nanodiscs at 3.7 Å resolution (orange density, 0.02 contour). (B) Cryo-EM structure of

732 ABCA7_{EQ-ATP} shown in ribbon format with half 1 and half 2 colored yellow and orange,

733 respectively. The transparent orange oval demarcates the observed exit pocket. (C) Central slice

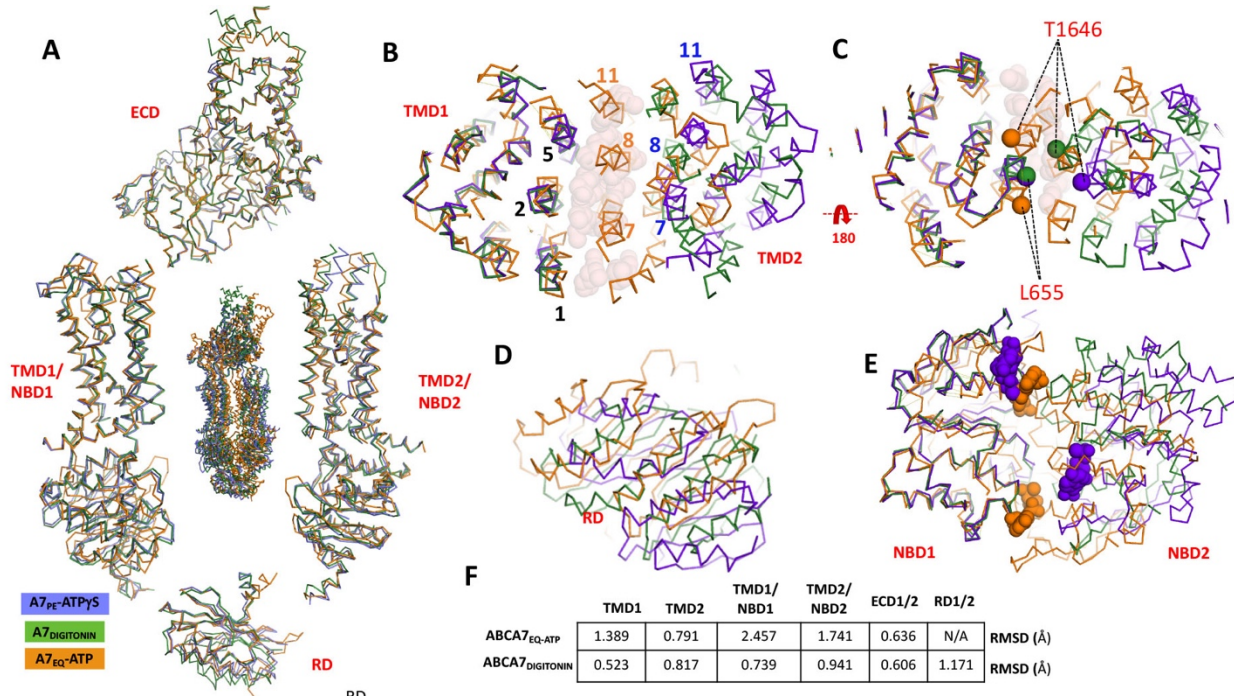
734 of electrostatic surface map showing surface details of exit pocket in two different orientations (D)

735 4-TM bundle forming the exit pocket. (E) NBDs viewed from the extracellular side with density

736 for bound nucleotide (blue sticks) shown in blue (0.02 contour).

737

738



739 **Figure 4. Comparison of open and closed conformations of ABCA7** (A) Overall structural

740 alignment of the three ABCA7 conformations (center) along with individual alignments of rigid

741 body pairs TMD1-NBD1, TMD2-NBD2, ECD, and RD (B) Overall alignment of the three ABCA7

742 conformations showing only TMD1 and TMD2 viewed from the extracellular side using the

743 TMD1-NBD1 pair as an alignment reference. TMs lining the TMD pathway are numbered (C)

744 Same as panel B, viewed from the cytoplasmic side with Ca atoms of gate forming residues shown

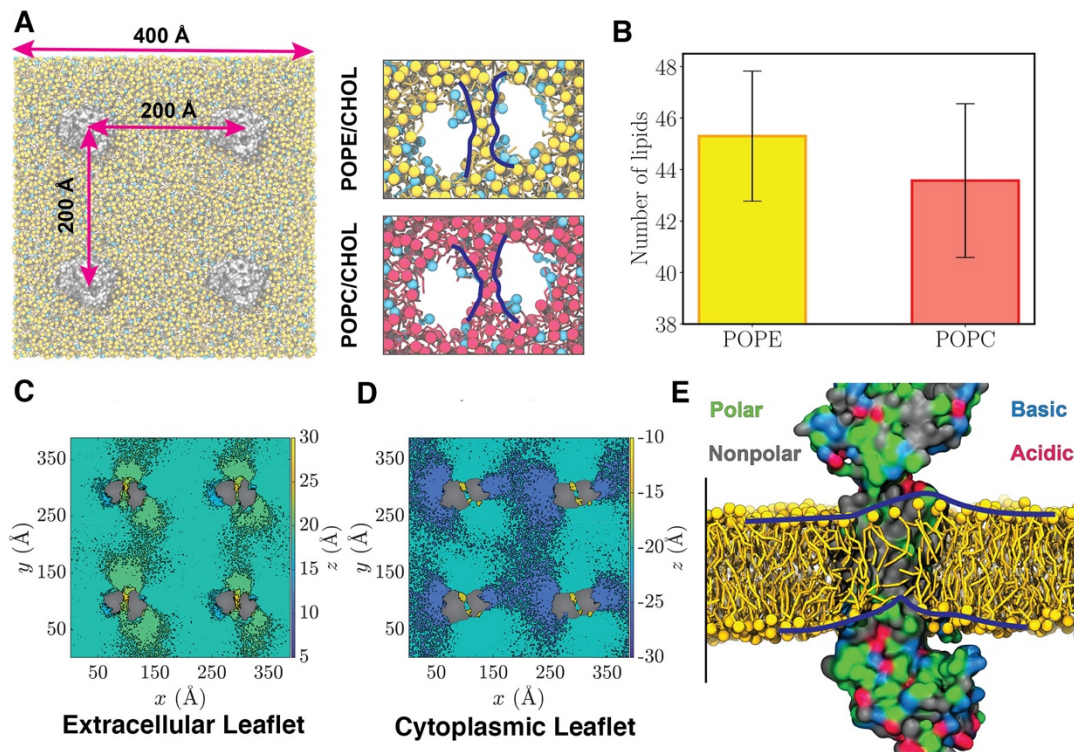
745 as spheres (D) Same as panels B/C showing only RDs viewed from the cytosolic side. (E) Same

746 as panel D showing just NBDs and bound nucleotides viewed from the extracellular side. ATPγS

747 and ATP-Mg²⁺ are shown as purple and orange spheres, respectively. (F) Root mean square

748 deviations (RMSD) of aligned atoms of ABCA7_{BPE} vs ABCA7_{EQ-ATP} and ABCA7_{DIGITONIN}.

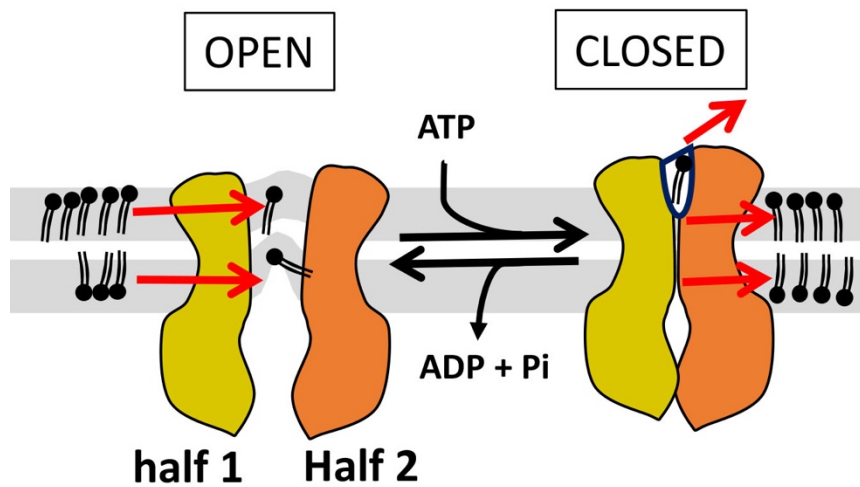
749



750 **Figure 5. MD Simulations of ABCA7 in Lipid Bilayers.** (A) Left: A representative simulation
 751 system with four copies of ABCA7 (silver), taken from the POPE/cholesterol (yellow/cyan) lipid
 752 patch. Right: the phospholipid belt (blue lines) formed in (top) the POPE/cholesterol (yellow/cyan)
 753 and (bottom) POPC/cholesterol (red/cyan) membranes ($t = 2 \mu\text{s}$). (B) The total count of
 754 phospholipids (sum of all four simulated proteins in a patch) partitioned in the TMD lumen for
 755 POPE/cholesterol and POPC/cholesterol bilayers (averaged over time \pm standard deviation). (C/D)
 756 Heatmaps representing the average height (z values) of POPE headgroup with respect to the
 757 membrane midplane in the extracellular (C) and cytoplasmic (D) leaflets. Phospholipids are
 758 observed to climb the protein and form a dome-like configuration in the TMD lumen. (E) Snapshot
 759 of lipids partitioned in the TMD lumen, taken from the POPE trajectory at $t = 2 \mu\text{s}$. Polar, nonpolar,
 760 basic, and acidic residues are colored green, gray, blue, and red, respectively. TMD2 is hidden for
 761 a clearer view of the luminal dome-like lipid configuration (outlined by blue lines).

762

763



764

765 **Figure 6. Proposed model of ABCA7 conformational transitions and lipid interactions.** The
766 membrane bilayer leaflets are shown in grey. Red arrows indicate movement of lipids (black)
767 under the influence of TMD conformation. The ECD and RD have been omitted for simplicity as
768 has any reference to potential lipid flipping from the cytoplasmic to extracellular leaflets.

769

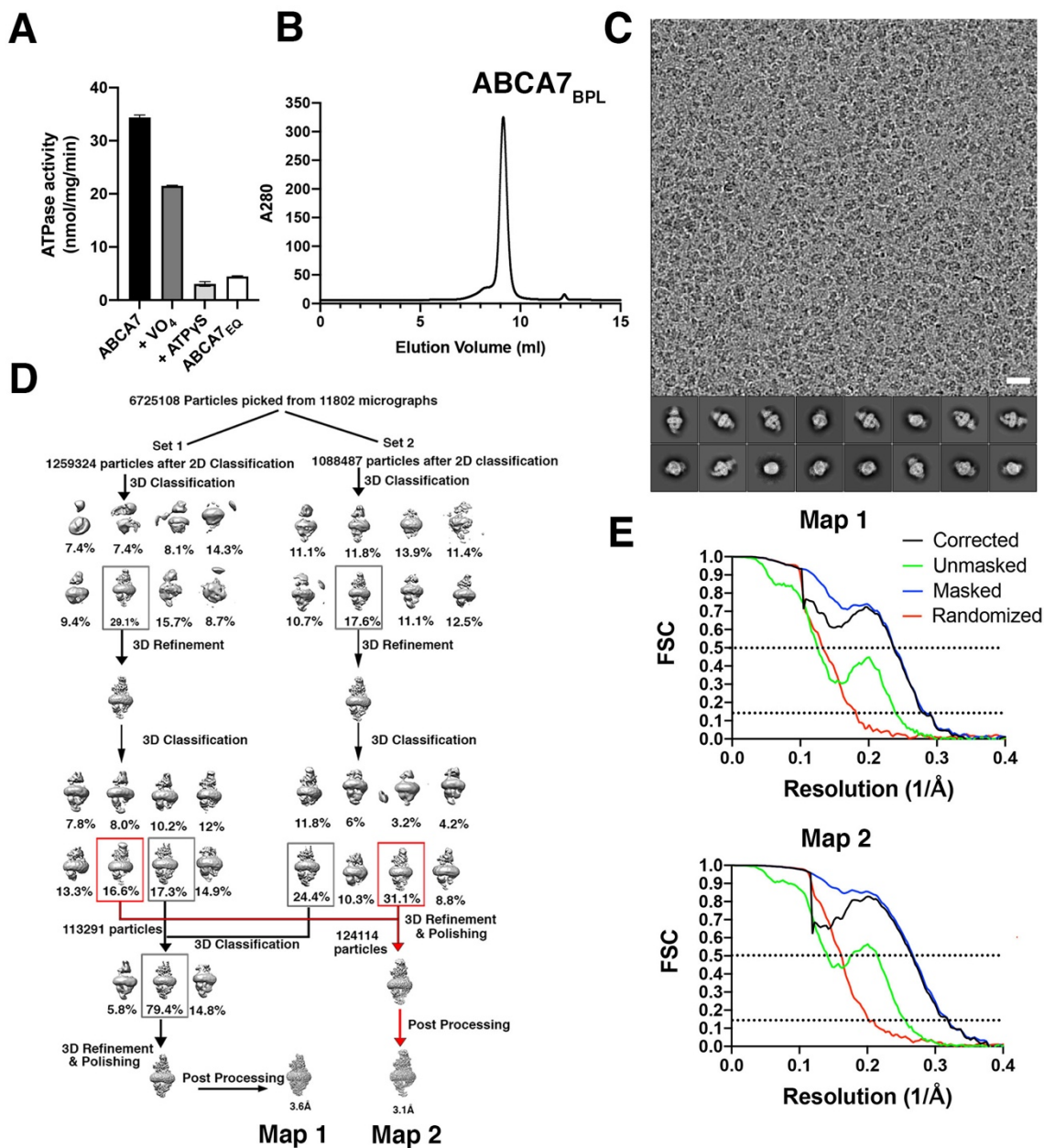
770

771

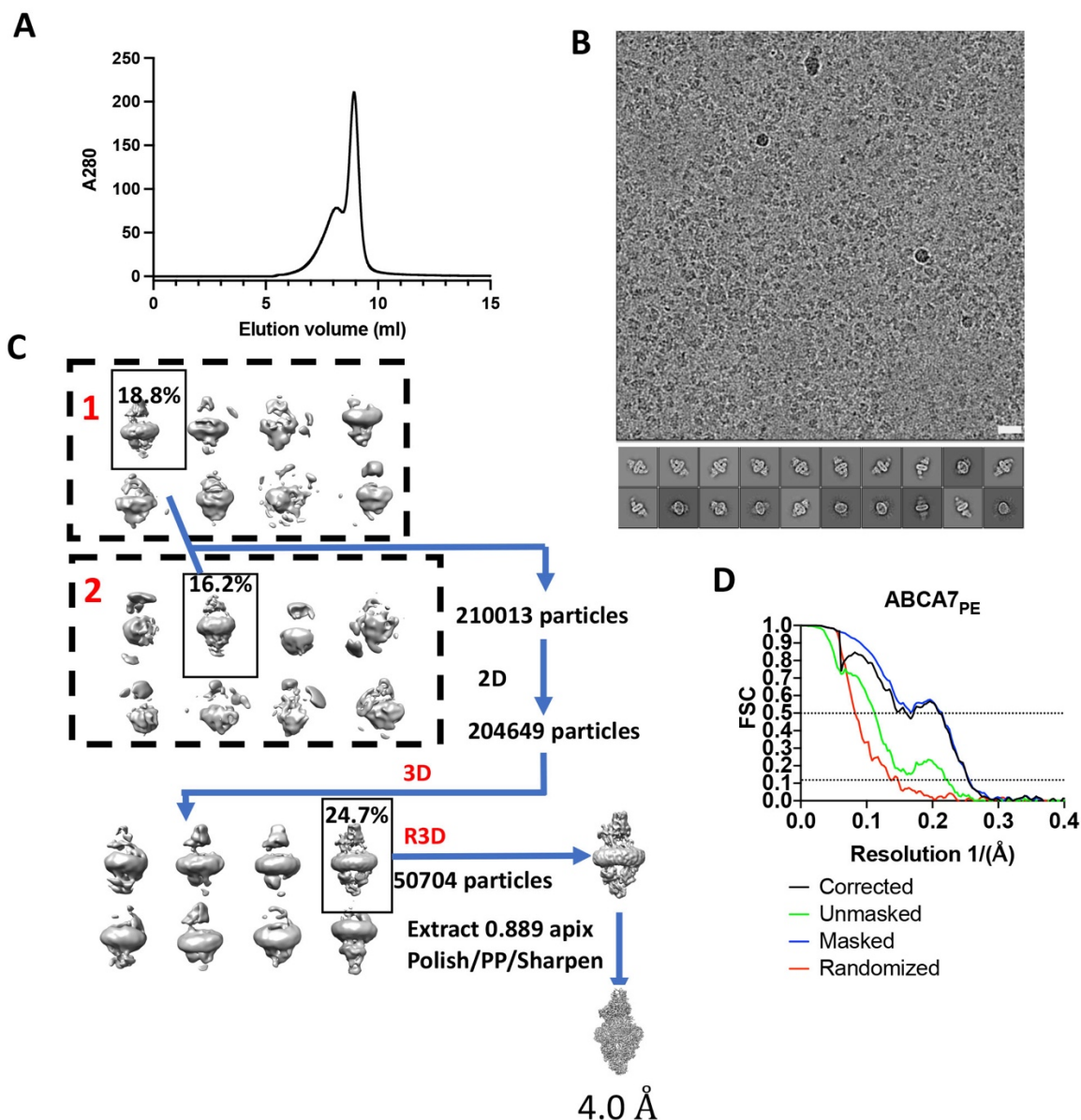
772

773

774

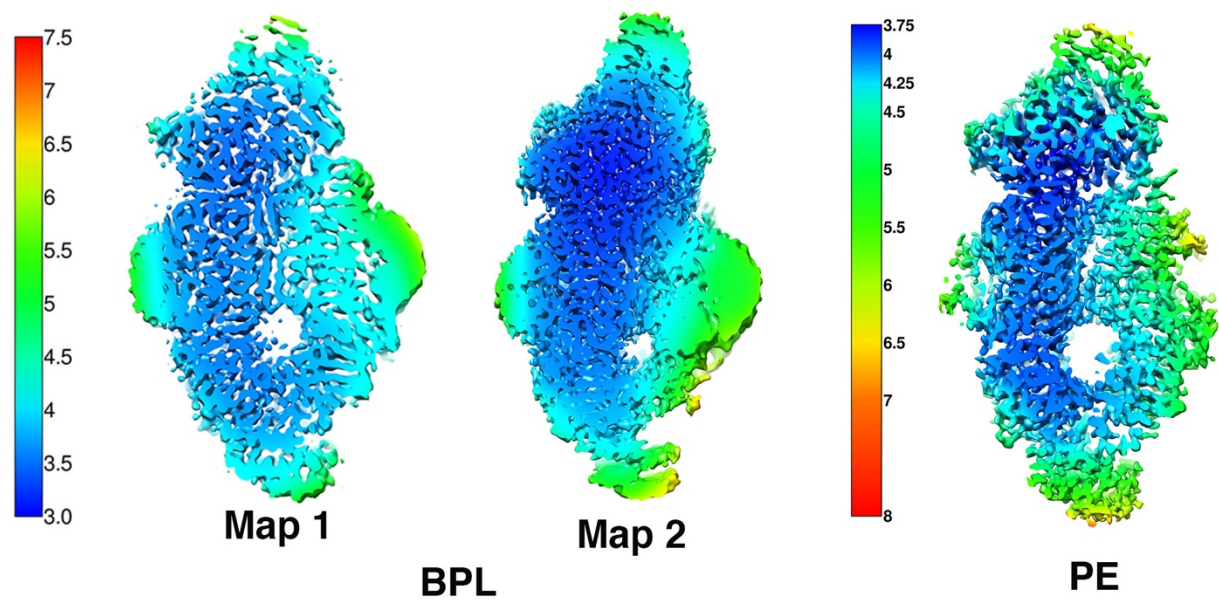


775 **Figure S1. ABCA7_{BPL} characterization and Cryo-EM data processing.** A ATPase data for
 776 nanodisc reconstituted ABCA7 with and without sodium orthovanadate (VO₄) or ATP γ S. N=3
 777 and error bars represent s.d B SEC peak of ABCA7_{BPL} sample for cryo-EM. C Representative cryo-
 778 EM micrograph at -2.5 μ m defocus. Scale bar = 20 nm. D cryo-EM processing workflow. Boxes
 779 indicate 3D classes used for further refinement for both Map 1 and Map 2 (red). E Fourier shell
 780 correlation (FSC) curves for Map 1 (top) and Map 2 (bottom) Dotted lines indicate position 0.143
 781 and 0.5 cutoff criteria for resolution estimates.



782

783 **Figure S2. ABCA7_{PE} Cryo-EM data processing.** **A** Size exclusion chromatography micrograph
784 of cryo-EM sample showing monodisperse ABCA7_{PE} nanodisc (main peak). **B** Representative
785 micrograph at -2.5 μm defocus and 2D classes. Scale bar = 20 nm. **C** cryo-EM processing
786 workflow. Dashed boxes demarcate Subsets 1 and 2. Solid boxes indicate 3D classes used for
787 further refinement. C2D = 2D Classification, C3D=3D classification, R3D = 3D refinement **D**
788 Fourier shell correlation (FSC) curves for ABCA7_{PE}. Dotted lines indicate position 0.143 and 0.5
789 cutoff criteria for resolution estimates.

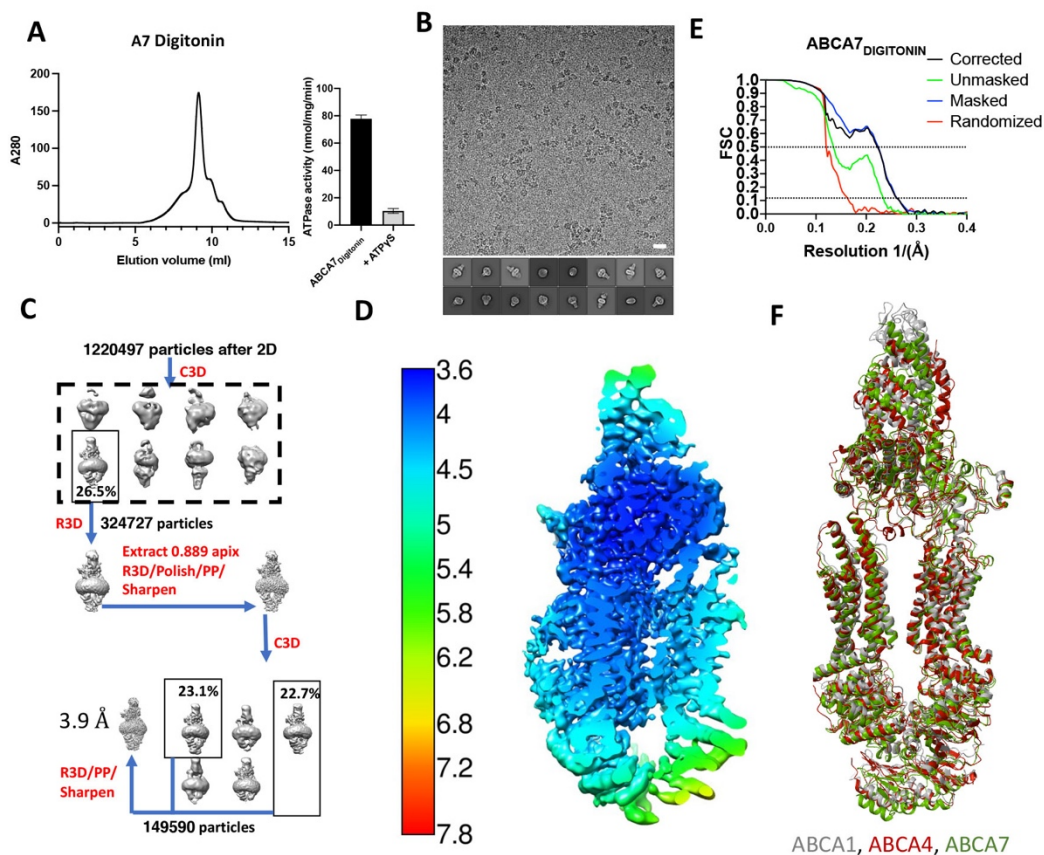


790

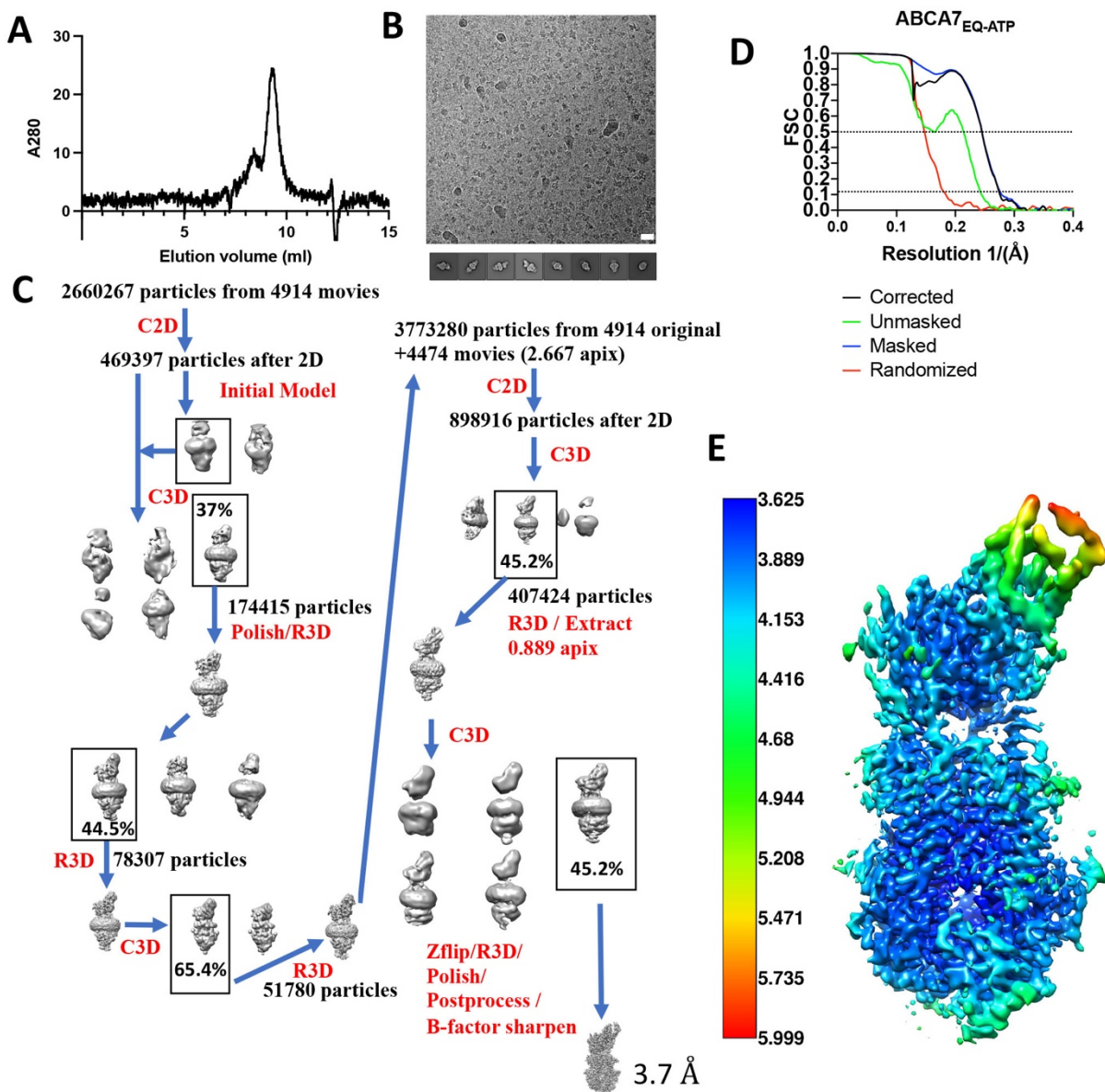
791 **Figure S3. ABCA7_{BPL} and ABCA7_{PE} local resolution filtered maps.** Color keys are indicated

792 on the left of each set of maps with numbers representing resolution (Å).

793



794
 795 **Figure S4 ABCA7_{DIGITONIN} cryo-EM processing** A SEC profile of ABCA7_{DIGITONIN} and its ATPase
 796 activity with and without ATPγS. B Representative micrograph at -2.5 μm defocus and 2D classes.
 797 Scale bar = 20 nm. C cryo-EM processing workflow. C2D = 2D Classification, C3D=3D
 798 classification, R3D = 3D refinement. D Local resolution colored EM map of ABCA7_{DIGITONIN}. E
 799 Fourier shell correlation (FSC) curves for ABCA7_{DIGITONIN}. Dotted lines indicate position 0.143
 800 and 0.5 cutoff criteria for resolution estimates. F Superposition of ABCA7 (green, this manuscript),
 801 ABCA1 (grey, PDB 5XJY), and ABCA4 (red, PDB 7LKP) structures in digitonin.
 802



803

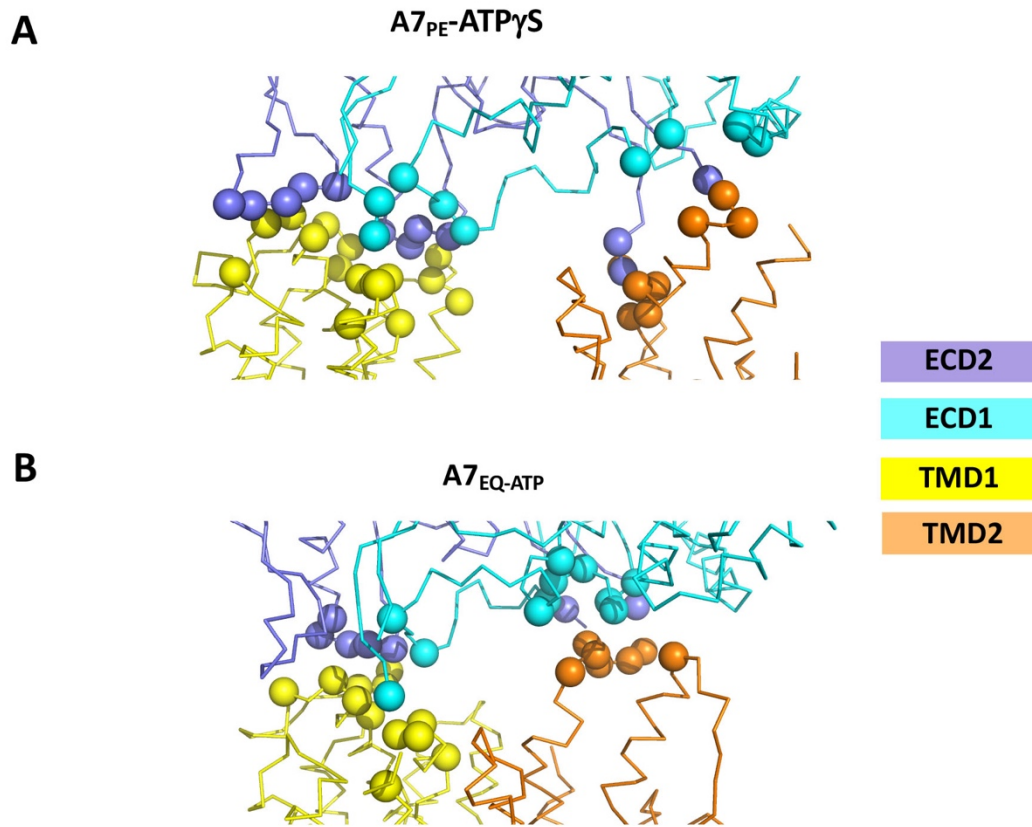
804 **Figure S5. ABCA7_{EQ-ATP} cryo-EM processing.** (A) SEC peak for ABCA7_{EQ-ATP} in nanodiscs. **B**

805 Representative EM micrograph (-2.5 defocus) and rep 2D classes for ABCA7_{EQ-ATP} sample. **C**

806 Cryo-EM data processing pipeline. C2D = 2D Classification, C3D=3D classification, R3D = 3D

807 refinement. **D** FSC curves. **E** Local resolution colored EM map.

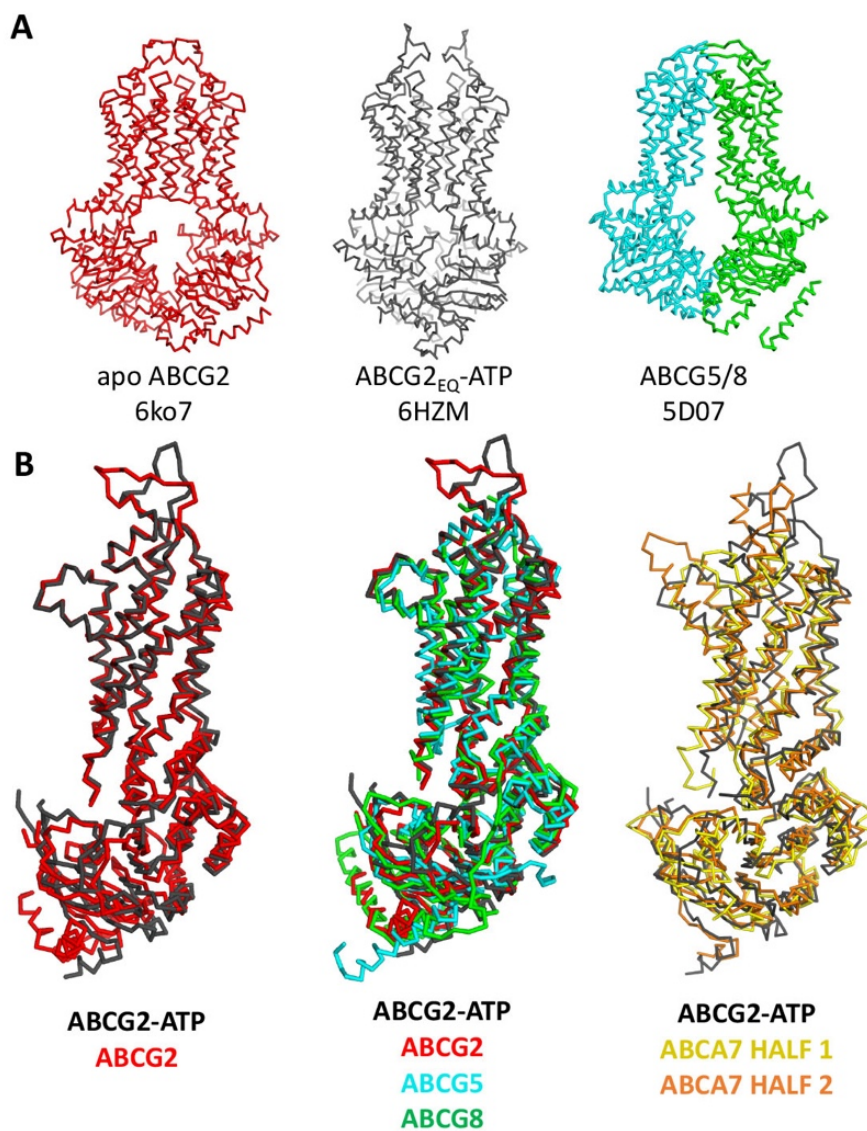
808



809

810 **Figure S6. TMD-ECD interfaces of open and closed form ABCA7.** (A) The TMD-ECD binding
811 interfaces of ABCA7_{PE} with TMD1 and TMD2 and with C α for residues in TMD1 and TMD2
812 within 5Å of either ECD or vice versa shown as spheres. (B) The same analysis for the TMD-ECD
813 binding interfaces of ABCA7_{EQ-ATP} with closed cavity.

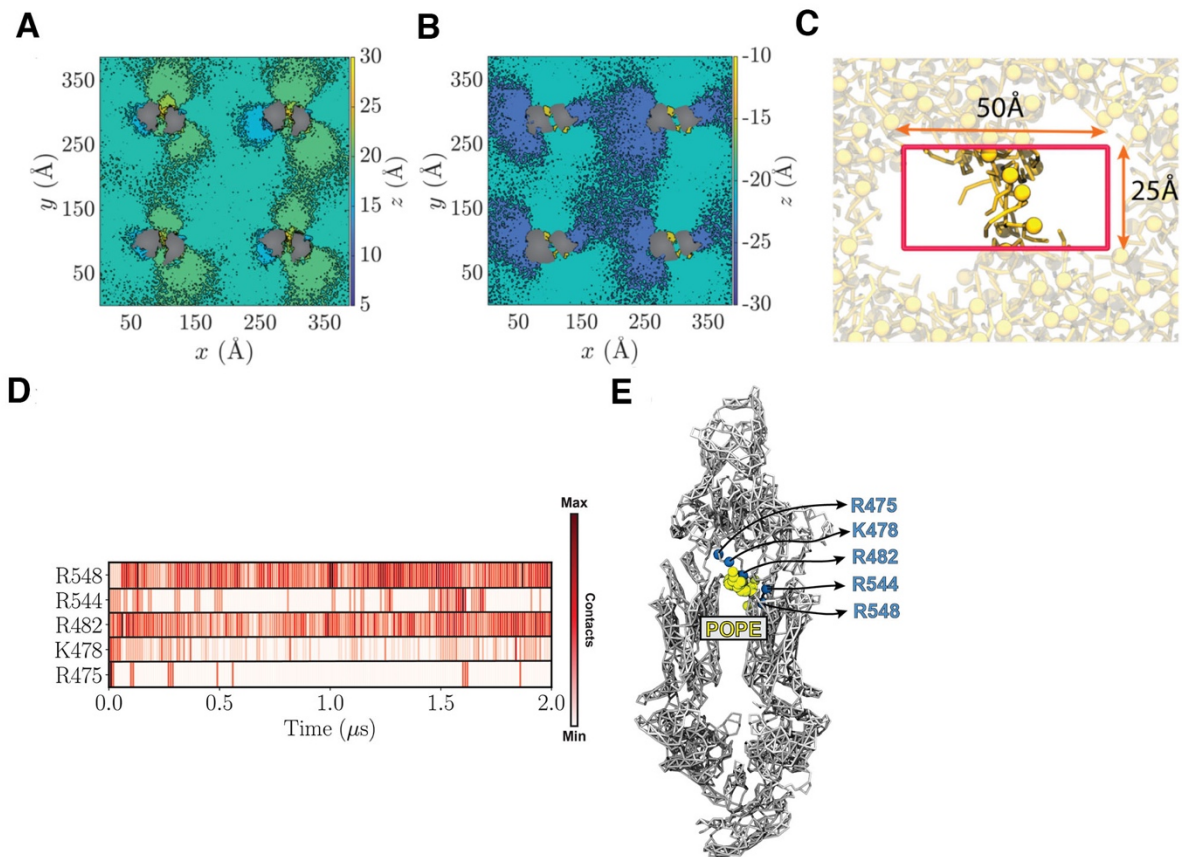
814



815

816 **Figure S7. Conservation of ABCA and ABCG family structural elements** (A) Ribbon
817 representation of select ABCG family transporter structures and their respective PDB IDs
818 including apo open ABCG2 (red), closed ATP bound structure of ABCG2_{EQ} (black), and
819 ABCG5/G8 (cyan and green, respectively) (B) Alignment of NBD-TMD pairs from open and
820 closed conformations of ABCG2 (left), ABCG2 and ABCG5/G8 (center), and closed ABCG2 with
821 TMD-NBD pairs from ABCA7 half 1 (gold) and half 2 (orange).

822



823

824 **Figure S8. Lipid configuration induced by protein copies in a POPC bilayer and criteria used**

825 **for identifying luminal lipids in MD simulations. (A/B)** POPC headgroup height calculated for

826 extracellular (A) and cytoplasmic (B) leaflets. (C) Dimension and position of the box used to

827 calculate the number of phospholipids (yellow) partitioned in the TMD leaflets. The box is

828 centered at the protein center and has dimensions of 50 Å and 25 Å in *x* and *y* directions,

829 respectively. The ABCA7 transporter is hidden for clarity. (D) Contact map, based on the number

830 of POPE headgroups in proximity of each residue throughout the simulation. (E) Accumulation of

831 POPE headgroups (yellow spheres) in close proximity of most frequently contacted residues

832 throughout the simulation.

833

834

hsABCA7 1 MAFWTQIMLLLWKNFMYRRRQIPVQLLVELELWPLFTFFLVAVRHSHPLEHECHFPNKPLPSAGTVPWL
 hsABCA1 1 MACWPOLRLLLWKNLTFRRRQITCQLLLEVAWPLFTFFLISVRLSYPPYEQHECHFPNKAMP SAGTVPWV
 hsABCA4 1 MGFVRQLQLLWKNWTLRRRQKIRFVVELEWPLSIFLVLWLRNANPLYSHHECHFPNKAMP SAGTVPWL

hsABCA7 71 QCIICNVNNTCFPQLTPGEBPCRLSNFNSLIVSRILADARTVGGASAHRTAGTGKLTATTRA.....
 hsABCA1 71 QCIICNANNPCFRYPTPGEBPCVVGNFNKSIVARLFS DARRLLYSQKDTSMKDMRKVLRTRQQI.....
 hsABCA4 71 QCIICNVNNTCFPQSPTPGESPCIVSNYNSILARVYRDFQELLMNAPESQHLGRITWTELHIISQFMDTLR

hsABCA7 135ARSTAQPOPTKQSPLEPPMLDVABTLTSLRTRTESL.
 hsABCA1 136KSSSNLKLQDFLVDNETFSGFLYHNLSPKSTVDKMLRADVILHKVFLQGYOHLTSL.CNGSKS
 hsABCA4 141 THPERIAGRGIRIRDILKDEETLTLFLIKNIGLSDSVVYLLINSQVRPEQFAHGVPDLAKDTIACSEALL

hsABCA7 170G LALGQAQ.....EPLHSTLEA
 hsABCA1 201 EEMIQLGDAQEVSE....LCGLPREKLA AAEVLRSNMDILKPI LR TLNSTSPFPSEKEL.AEATKTLLHS
 hsABCA4 211 ERFIIFSQRRAKTVRYALCSLSQGTLOWIEDTLYANVDFFK.LFRVLP TLLDSRSQGINLRSWGGTLLSD

hsABCA7 187 AEDLLOE L LALRSLVFLRALLQRPRGTSGP.....LELLESEALC SVRGSSTVGPSTLWYFA S DLMELV
 hsABCA1 265 LGLLLOE LFSMR SWSDMRQEVMLFNVNSSSSSTQIYQAVSRIVCGHPEGGLKIKS L WYFD N NYKALF
 hsABCA4 280 MSPRLOE F IHRP SMQDL L WVT R L M Q N G G P E T F T K L M G L L S D L L C G Y P E G G G S R V L S F N W Y E D N N Y K A F L

hsABCA7 251 C...QEPESALPDS S L S P A C S E L T G A L D S H P L S R L L W R R L K P L I L G K I L F A P D T P F T R K L M A Q V N R T F E
 hsABCA1 335 CNGTEEDAETFYDNSTTPYCNLDL MKNLES S PLSRIIWRAL K P L L V G K I L Y P D T P A T R Q V M A E V N K T F Q
 hsABCA4 350 CIDSTRKDPIYSYDRRTTSCNALIQSLESNPLTKIAWRRAKPLLMGKILYTPDSPAARRILKNANSTFE

hsABCA7 317 ETL L L R D V R E V W E M L G P R I F T F M N D S S N V A M I Q R L L Q M Q D E G R R Q P R P G G R D H M . . E A L R S F L D P G . . .
 hsABCA1 405 E L A V F H D L E G W E E L S P K I N T F M E N S Q E M D L V R M L L D S R D N D H F W E Q Q L D G L D W T A Q D I V A F L A K H P E D V
 hsABCA4 420 E L B H V R K L V K A W E E V G P Q I M Y F F D N S I Q M M I R D T L G N P T V K D F L N R Q L G E E G I T A E A L L N F L Y K G P R E S

hsABCA7 381 ...SGGYSWQDAHADVGHLVGT LGRVT ECLSLDKLEAAPS E A A L V S R A L Q L L A E H R F W A G V V F L G P E D S
 hsABCA1 475 QSSNGSVYTWREAFNETNQAITRTISRFM ECVNLNKL E P I A T E V W L I N K S M E L L D E R K F W A G I V F
 hsABCA4 490 QADDMANFWDRI FNITDRTLRLVNQYL ECLVLDKFE SYNDE T Q L T Q R A L S L L E N M F W A G V V F

hsABCA7 447 SDPTEH L T P D L G P G H V R I K I R M D I D V V T R T N K I R D R F W D P G P A A D P L T D L R Y V W G G F V Y L Q D I V E R A A V R
 hsABCA1 539 . . T G I T P G S I E L P H V K Y K I R M D I D N V E R T N K I K D G Y W D P G P R A D P F E D M R Y V W G G F A Y L Q D V V E Q A I I R
 hsABCA4 554 . . P D M Y E W T S S L P H V K Y K I R M D I D V V E K T N K I K D R Y W D S G P R A D P V E D F R Y E W G G F A Y L Q D M V E Q G I T R

hsABCA7 517 VLSGANPRA G Y L Q Q M P Y P C V V D D V F L R V L S R S L P L F L T L A W I Y S V T L T V K A V V R E K E T R L R D T M R A M G L
 hsABCA1 607 VLTGTEKKT G V Y M Q Q M P Y P C V V D D I F L R V M S R S M P L F M T L A W I Y S V A V I I K G I V Y E K E A R L K E T M R I M G L
 hsABCA4 622 S Q V Q A E A P V G Y L Q Q M P Y P C V V D D S F M I L L N R C P I F M V L A W I Y S V S M T V K S I V L E K E L R L K E T L K N Q G V

hsABCA7 587 SRAV L L V L G W F P S C L G P F L L S A A L L V L V L K L G D I L P Y S H P G V V F L F L A A F A V A V T Q S F L S A F F S R A N L A
 hsABCA1 677 D N S I L W F S W F I S S L I P L L V S A G L L V V I L K L G N L L P Y S D P S V V F V F L S V F A V V T I L Q C F L I S T L F S R A N L A
 hsABCA4 692 S N A V I W C T W F E D S F S I M S M S F L L L T I F I M H G R I L H Y S D P F I L F L L A F E S T A T I M L C F L S F F E S K A S L A

hsABCA7 657 AACGGLAYFSLYLPYVLCVAVRDRIPAGGRVAASLLSPVAFGFGCESLALLLEQGECAQWNNVGTRET.A
 hsABCA1 747 AACGGIIFYFLYLPYVLCVAVQDYVGFITLRFASLLSPVAFGFGCEYFALFEEQIGVQWQNIIFESDVEE
 hsABCA4 762 AACSGVIYFFLYLPHLFCFAVQDRMTAEELKASLLSPVAFGFGTEYLVRFEQGLCHQWSNIGNSRTEG

hsABCA7 726 DVFSLAQVSGLLLDAALYGLATWYEAQVPCQYGIPEPWFPPFRRSYWCGLD.....PRPKSPAFCP
 hsABCA1 817 DGFNLTTSVSMMLLDFLFDLYGVMTWYEAQVPCQYGIPEPWFPPFRRSYWCGLD.....EESDEKSHPGS
 hsABCA4 832 DDFSLFLSMQMLLDAAVYGLLAWYLDQVPCQYGIPEPWFPPFRRSYWCGLD.....GEGCSTREREALKEKTEPLT

hsABCA7 788 TPLD.....PKVLVEEAFPPGLSPGVSVRSLEBRFPFGSPQPALRGLSLDFYQGHITAFGLHNGAGKTT
 hsABCA1 879 NQKR.....ISEICMBEEPTHLLKLVSVIQNLVQVYRDGMKVAVDGLALNFMEGQITSPFLHNGAGKTT
 hsABCA4 902 EETEDPEHPEGIHDSFFEREHPGWVPGVGVKNLVKRFEPFCGRPAVDRLNITFYENQITAFGLHNGAGKTT

hsABCA7 850 TMSILSGLFPFSGSALFLCHDVRSSMAATRPHLGVCPQYNNVLEDMLTVDHEVWFYGRKGLSAAVVGPE
 hsABCA1 942 TMSILTGLFPFSSGTAYILCKDIRSEMSTRQNLGVCPQHNVLEDMLTVEEHLWFYARLKGISEKHVKAE
 hsABCA4 972 TMSILTGLLFPFSSGTAYILVGRDIETSLDVRQSLGMCPQHNLVLEHHLTVAEHMLFYAQLKGRKSEEAQLE

hsABCA7 920 QPRLLODVLCLVSKQSVQTRHLSGGMORKLSVAFAFVGGSQVVLDEPTAGVDPASRRGIWELLLKYRQC
 hsABCA1 1012 MEGMALDVLCLPSSKLSKTSQLSGGMORKLSVAFAFVGGSKVVLDEPTAGVDPYSSRRGIWELLLKYRQC
 hsABCA4 1042 MEGMLDVLCLVSKRNEEAQDLSGGMORKLSVAFAFVGGDAKVVLDEPTAGVDPYSSRSIWELLLKYRQC

hsABCA7 989 RTIILSTHHLDEAELGDRVAVVAGGRLLCGSGSLFLRRLHLSGGLYTLTVKARLPLTTNEKADTDMEGSV
 hsABCA1 1082 RTIILSTHMDLDEADVLGDRVAVVAGGRLLCGSGSLFLRRLHLSGGLYTLTVKARLPLTTNEKADTDMEGSV
 hsABCA4 1111 RTIIMSTHMDLDEADVLGDRVAVVAGGRLLCGSGSLFLRRLHLSGGLYTLTVKARLPLTTNEKADTDMEGSV

hsABCA7 1059 DTRQEKKNQSGQSRVGTPO.....LLALVQHWPGLARLVEELPHETVVLVLYTGAAHDGSAFATL
 hsABCA1 1152 LKKEEDSVSQSSDAGLSDHESDITLIDVSAISNLIRKHWSEARLVEDIGHEITVLYEAAKKEGAVVEL
 hsABCA4 1180 SSKGFSTLCPAHVDDLTPEQVLDG...DVNELMDVVLHWPGLARLVEELPHETVVLVLYTGAAHDGSAFATL

hsABCA7 1117 FRELDTRLAELRLTGYSISDTSLLEIFLKVVEECAADTMEDGSC.GQHLCTGIAGLDVTLRLKMPPEET
 hsABCA1 1222 FREIDDRLSDLGISSYGISDTSLLEIFLKVVAEESGVDAETSDECTLPARRNRRAFGDKQSCLRPFTEDDAA
 hsABCA4 1247 FRELEETLADLGLSISDTSLLEIFLKVTEDESDSGPLFAGC...AQQKRENVNPRHPCLP.REKAGQ

hsABCA7 1186 ALENGEPAGSAPETDQGSGL...PDAVGL.RVQCWALTRQQLQALLKRFLLARSRRLGFAQIVLPAL
 hsABCA1 1292 DPNSSDIDPESRETDLLSCM...DGKGSYQVKWKLQOQFVALLNKRLLIARRSRKGFRAQIVLPVAV
 hsABCA4 1313 TPQDSNVCSPGAPAAHPEQPPPEPECPQPQLNTCTQLVQLHVQALLVKKRFQHTIRSHKDFLAQIVLPAT

hsABCA7 1249 FVGLALVFSLLVPPFCHYPALRLSPTMYGAQVSEFSEDAFGDPGRARLLEALQEA.....LEE
 hsABCA1 1357 FVCIALVFSLLVPPFCKYPSDELQDWMYNEQYTFVSNDAPEDEGTGLELINALTKDPCFGTRCMENPIP
 hsABCA4 1383 FVFLALMLSIYVPPFCHYPALRLSPTMYGAQVSEFSEDAFGDPGRARLLEALQEA.....LEE

hsABCA7 1309 FVQVHSSHRFSAPEVPAEVAKVLASGNWTPESPSPACCCSRPGARRLLEDCPAAAGCFPPQAVTGSSEV
 hsABCA1 1427 TPCQAGEEETITAPVPTIMDLFQNGNWMQNPSPACCCSSDKIKKMLFVCPFGAGLPPPOKQNTADI
 hsABCA4 1453 YBC.GNSTPMTKTPSVSPNITQLFQKQWTVQVNPSPACCCSREKRLMLECEPAGGLPPPOKQNTADI

hsABCA7 1379 VQNLTGRLNSDFLVKTYPRLVROGLTKKRWVNEVRYGGFSLGGRDP.GLPSSGQELGRSVEELWALSPLP
 hsABCA1 1497 LQDLTGRNLSDFLVKTYVQIIRAKSLKNKRWVNEVRYGGFSLGVSNTQALPPSQEIVNDALIKQMKKHLKLA
 hsABCA4 1522 LQDLTGRNLSDFLVKTYPALIRSSLKSFRWVNEVRYGGFSLGKLPVVPITGEALLVGFLLSDLGRIMNVSG

hsABCA7 1448 GGALDRVLKNTAWAHS LDAQDSLKTFWNNKGWHSMVAFVNRASNAILRAHLPPGPARHAHSITTLNHPL
 hsABCA1 1567 DSSADRFNLNLSGRFMTGLDTKNNVWVFNKKGWHAISSFLNVINNAILRANLQKGENPSHYGTTAFNHPL
 hsABCA4 1592 GPITREASKEIFDFLKHLETEDNIKVWVFNKKGWHALVSLNVAFNAILRASLPKDRSPPEEYGTTVISQPL

hsABCA7 1518 NLTKEQLSEGLMAGSVDVIVSICVVFAMSFVPASFVLIQERVTRAKHLOLMGGLSPTLYWLDGNFLWD
 hsABCA1 1637 NLTKEQLSEVALMTISVDVIVSICVVFAMSFVPASFVLIQERVSKAKHLOFISGVKRPVIYWLNSNFVWD
 hsABCA4 1662 NLTKEQLSEITVLTISVDAVVAICVVFAMSFVPASFVLIQERVNKS KHLOFTISGVSPTTYWVTFNFLWD

hsABCA7 1588 MGNVLYVACIVVLIIFLAFOQRAYVAPANLPAALLLLLYGWSITPLMYPASFFSVPSTAYVVLTCINLF
 hsABCA1 1707 MGNVYVBPATLWIIIFICFOOKSYVSSSTNLVLAALLLLLYGWSITPLMYPASFFKIPSTAYVVLTSVNLFF
 hsABCA4 1732 LKNYSVSAAGLVVGIIFLGFOKRAYTSPENLPAALLLLLYGWAIVPLMYPASFFDVPSTAYVVALSCANLF

hsABCA7 1658 IGINSGNATFVLELFSQKIQEVSRIILKQVFLIFPHFCLGRGLDMVNRNOAMADAFERLCLRQFQSPFLR
 hsABCA1 1777 IGINSGVATFVLELFTDNKLNININDILKSVFLIFPHFCLGRGLDMVNRNOAMADALERFQENRFRSPLS
 hsABCA4 1802 IGINSSAIFVLELEFNRTLRFNAVLRKLLVFPFHCLGRGLDLALSOAVTDVYARFGEHSAIPLFH

hsABCA7 1727 WEVVGKRLAMVIQGLFLFLITLLHQHRSQLLPQPRVRSPLPLGEEDEDDVAREERVVQGATQGDVIVLRL
 hsABCA1 1846 WDLVGRNLFAMAVEGVVFFLITVLLQYRFFIRRPVNAKLSPLNDEDDVRRERQRIIDGGGQNDVFEIK
 hsABCA4 1872 WDLIGKRLFAMVVEGVVYFLITLLVQRHFFLSQWIAEPTKEPLVDEDDVAREQRIITGGNKTDITRLH

hsABCA7 1797 NLTKKVYRGQRMFAVDRIQLCFPGECFGLLGVNGACKTSTFRMVTGDTLASRCEAVLAGHSVIREPSAAH
 hsABCA1 1916 ELTKIYRKRKFAVDRIQVCFPGECFGLLGVNGACKSSTFKMVTGDTTVTRCDALFNKNSILSNHEVH
 hsABCA4 1942 ELTKIYPGTSSFAVDRLCVGWRPGEFCFGLLGVNGACKTSTFRMVTGDTTVTSQDATVAGKSIITNISEVH

hsABCA7 1867 LSMGYCPOSDAIFELLTGREHLELLARLRGVPEAQVAQTAGSGTARLGLISWYADRPAGTYSGGNKRRLAT
 hsABCA1 1986 QSMGYCPOFDAITELLTGREHVEFVALLRGVPEKEVGVKVGEWALRKLGLVVKYGEKYAGNYSGGNKRRLST
 hsABCA4 2012 QSMGYCPOFDAITELLTGREHLYLYARLRGVPAEEIEKVANWSLKSGLITVYADCLAGTYSGGNKRRLST

hsABCA7 1937 AALALVCDPAVVFLEDEPTTGMDPSARRFLWNSLLAVVREGRSVMVLTSHSMEECEALCSRLAIMVNGRFRCL
 hsABCA1 2056 ANALIGCPVVFLEDEPTTGMDPKARRFLWNCALSVVKEGRSVMVLTSHSMEECEALCRLAIMVNGRFRCL
 hsABCA4 2082 AALALIGCPVVFLEDEPTTGMDPQARRMLWNVIVSIIREGRAVVMVLTSHSMEECEALCRLAIMVKGAFRCM

hsABCA7 2007 GSPQHLKGRFAAGHTITLRVPAAR.....SQPAAAFVAAEFPGAELREAHGGRLRFQLPPGGRCALARV
 hsABCA1 2126 GSVQHLKNNRFQDGYTIVVRIAGSN.....PDLKPVQDFGLAPEGVLRKRRNMLQYQLP.SSLSSLARI
 hsABCA4 2152 GTIQHLKSKFQDGYITVTKIKSPKDDLPLDLPVEQFFQGNFPGSVQRERHYNMLQEQVVS.SS.SLARI

hsABCA7 2071 FGE LAVHGAEHGVDEFSVSTMLEBVFLYSKDQ GKDEDETEEQKEAGVGVDPAPGLQHPKRVSQFLDDPS
 hsABCA1 2191 FSI LSQSKRRLHIEDYSVSTMLDQVFNBAKQSDDDHLKD.....LSLHKNTVVVDVAVLTSFLQDEK
 hsABCA4 2219 FQLLLSHKSDSLIEEYSVSTMLDQVFNBAKQTESH.....D.....LPLHPRAAGASRQAQD.....

```
hsABCA7 2141 TAETVL  
hsABCA1 2256 VKESYV  
hsABCA4      . . . . .
```

848

849 **Figure S10 Sequence alignment of human (hs) ABCA7, ABCA1, and ABCA4.**

Dataset	ABCA7 _{BPL}		ABCA7 _{PE}	ABCA7 _{DIGITONIN}	ABCA7 _{EQ-ATP}
Magnification	96k		96k	96k	96k
Pixel Size (Å)	0.895		0.889	0.889	0/889
Total Dose (e/Å ²)	60		40	40	40
Defocus Range (um)	-0.8 to 2.6		-0.8 to 2.6	-0.8 to 2.6	-0.8 to 2.6
Maps	Map 1	Map 2	Map3	Map4	Map5
EMDB ID	EMD-22996	EMD-22998	EMD-A	EMD-B	EMD-C
# Particles in final Class	91381	124114	50704	149590	177230
Resolution (Å) (0.143 threshold)	3.6	3.2	4.0	3.9	3.7
Sharpening B factor					
Refined Coordinates	ABCA7 _{BPL}		ABCA7 _{PE}	ABCA7 _{DIGITONIN}	ABCA7 _{EQ-ATP}
PDB ID	AAAA		BBBB	CCCC	DDDD
# Residues/Non-hydrogen Atoms	1801/14761		1846/14749	1856/4662	1871/14748
Glycans	16		16	26	16
Ligands	21		20		2
R.M.S deviations					
Bond Length (Å)	0.003		0.003	0.003	0.003
Bond Angles (°)	0.616		0.600	0.678	0.645
MolProbity Statistics					
MolProbity Score	1.68		1.72	1.83	1.77
Clashscore	8.05		8.16	11.40	9.83
Poor rotamers (%)	0.00		0.00	0.00	0.00
Ramachandran statistics					
Favored (%)	96.38		95.84	96.24	96.22
Allowed (%)	3.62		4.16	3.76	3.78
Outliers (%)	0.00		0.00	0.00	0.00

850
851
852
853

Table S1 Data collection and refinement statistics.